



1 **Further improvement of wet process treatments in GEOS-Chem v12.6.0: Impact on global**
2 **distributions of aerosol precursors and aerosols**

3

4 Gan Luo¹, Fangqun Yu¹, Jonathan M. Moch²

5

6 ¹Atmospheric Sciences Research Center, University at Albany, Albany, NY, USA

7 ²Department of Earth and Planetary Sciences, Harvard University, Cambridge, MA, USA

8

9 **Abstract**

10 Wet processes, including aqueous phase chemistry, wet scavenging, and wet surface
11 uptakes during dry deposition, are important for global modeling of aerosol precursors and
12 aerosols. In this study, we improved the treatments of these wet processes in the GEOS-Chem
13 v12.6.0, including pH calculation for cloud, rain, and wet surface, fraction of cloud available for
14 aqueous phase chemistry, rainout efficiencies for various types of cloud, empirical washout by
15 rain and snow, and wet surface uptakes during dry deposition. We compared simulated surface
16 mass concentrations of aerosol precursors and aerosols with surface monitoring networks over
17 the United States, Europe, Asia, and Arctic regions, and showed that the model results with the
18 updated wet processes agree better with measurements for most species. With the
19 implementation of these updates, normalized mean biases (NMB) of surface nitric acid, nitrate,
20 and ammonium are reduced from 78 %, 126 %, and 45 % to 13 %, 24 %, and 6.2 % over US
21 sites, from 56 %, 105 %, and 91 % to -20 %, -5.1 %, and 22 % over Europe sites, and from
22 121 %, 269 %, and 167 % to -18 %, 40 %, and 86 % over Asia sites. Comparison with surface
23 measured SO₂, sulfate and black carbon at four Arctic sites indicated that these species simulated
24 with the updated wet processes match well with observations except large underestimation of
25 black carbon at one of the sites. Furthermore, we compared model simulation with aircraft
26 measurement of nitric acid and aerosols during ATom-1 and ATom-2 periods and found seasonal
27 variation and vertical profile of these species have been successfully improved by considering
28 the updated wet processes. The investigation of impacts of updated wet process treatments on
29 surface mass concentrations indicated that the updated wet processes have strong impacts on the
30 global means of nitric acid, sulfate, nitrate, and ammonium and relative small impacts on the
31 global means of sulfur dioxide, dust, sea salt, black carbon, and organic carbon.



1

2 **1. Introduction**

3 Aqueous phase chemistry, wet scavenging, and wet surface uptake during dry deposition
4 are the three major atmospheric wet processes for aerosols and aerosol precursors. Aqueous
5 phase chemistry plays a role as reaction chamber which efficiently converts aerosol precursors to
6 aerosols (Ervens et al., 2011; Walcek and Taylor, 1986). Wet scavenging, a process by which
7 chemicals accumulate in droplets and then are removed by precipitation, is the predominantly
8 removal pathway of aerosols and aerosol precursors (Textor et al., 2006). Dry deposition, where
9 chemicals settle out of the atmosphere in the absence of precipitation, is greatly enhanced due to
10 the absorption of water soluble gases at wet surfaces associated with dew, fog, and rain (Garland
11 and Branson, 1977; Wesely, 1989). These wet processes significantly impact global mass load
12 and redistribute aerosol precursors and aerosols. Since aerosol mass load and its global
13 distributions are important for the studies on aerosol optical properties (Kinne et al., 2006),
14 aerosol direct radiative forcing (Myhre et al., 2013; Penner et al., 1994), and particle matter's
15 health effects (Shiraiwa et al., 2017; Hopke et al., 2006), a better representation of wet processes
16 in global modeling of aerosol precursors and aerosols is important.

17 GEOS-Chem is a widely used community model which is continuously being improved
18 (Holmes et al., 2019; Keller et al., 2014; Martin et al., 2003; Bey et al., 2001). Luo et al. (2019),
19 L2019 thereafter, updated the GEOS-Chem wet scavenging scheme by using the Modern-Era
20 Retrospective analysis for Research and Applications, Version 2 (MERRA-2) spatially and
21 temporally varying cloud and rain water to replace the assumption of fixed in-cloud
22 condensation water (ICCW) in the GEOS-Chem rainout parameterization and by using new
23 empirical rates for nitric acid and water soluble aerosols in washout. These changes together
24 reduced the normalized mean biases (NMB) of simulated nitric acid, nitrate, and ammonium
25 mass concentrations at the United States' surface monitoring networks from 145 %, 168 %, and
26 81 % to 24 %, 25 %, and 13 %, respectively. However, the impacts of updated wet scavenging
27 scheme on the simulations over other regions (Europe, Asia, and remote areas) and free
28 atmosphere were not investigated. Moreover, L2019 only investigated the changes of nitric acid,
29 nitrate, and ammonium. The impact of updated wet scavenging scheme on other aerosols such as
30 sulfate, sea salt, dust, and carbonaceous aerosols were not investigated in that work. Due to the
31 large impact of updated wet scavenging on model simulations, a comprehensive validation of



1 simulated aerosol precursors and aerosols with ground based monitoring networks for surface
2 mass concentrations and aircraft measurements for vertical profiles is needed.

3 In this study, we further update the treatments of wet processes (aqueous chemistry, wet
4 scavenging, and wet surface uptakes during dry deposition) in GEOS-Chem and evaluate
5 comprehensively simulated major inorganic aerosol precursors (sulfur dioxide, nitric acid, and
6 ammonia) and aerosols (sulfate, nitrate, ammonium, black carbon, and organic carbon) by
7 comparison with a large set of in-situ observations. The updates to the wet processes are detailed
8 in Section 2. Comparisons of simulations with measurements from surface monitoring networks
9 including the United States Environmental Protection Agency (USEPA), the Interagency
10 Monitoring of Protected Visual Environments (IMPROVE), the Chemical Speciation Network
11 (CSN), the Clean Air Status and Trends Network (CASTNET), the Ammonia Monitoring
12 Network (AMoN), the European Monitoring and Evaluation Programme (EMEP), and the Acid
13 Deposition Monitoring Network in East Asia (EANET) are given in section 3.1. Validations of
14 aerosol precursors and aerosols at the Arctic and the Atmospheric Tomography (ATom) mission
15 are presented in sections 3.2 and 3.3. The impact of the updated wet processes on global surface
16 mass concentrations are discussed in section 3.4. A summary of our results is given in section 4.

17

18 **2 Updates of wet process treatments in GEOS-Chem associated with aerosol precursor and** 19 **aerosol modeling**

20 In the public released GEOS-Chem version 12.6.0, GC12 thereafter, aqueous phase
21 chemistry in cloud was developed by Chin et al. (2000) for SO₂. Wet scavenging scheme was
22 developed by Jacob et al. (2000) and Liu et al. (2001) for aerosols and by Amos et al. (2012) for
23 gases. Scavenging of aerosol by snow and cold-mixed precipitation was updated by Wang et al.
24 (2011, 2014). Wet surface uptakes during dry deposition is represented with constant values of
25 effective Henry's law coefficient for surface resistance calculation
26 ([http://wiki.seas.harvard.edu/geos-chem/index.php/Physical_properties_of_GEOS-](http://wiki.seas.harvard.edu/geos-chem/index.php/Physical_properties_of_GEOS-Chem_species#Definition_of_Henry.27s_law_constants)
27 [Chem_species#Definition_of_Henry.27s_law_constants](http://wiki.seas.harvard.edu/geos-chem/index.php/Physical_properties_of_GEOS-Chem_species#Definition_of_Henry.27s_law_constants)).

28 L2019 showed that the assumption of in-cloud condensation water with a fixed value (1
29 g·m⁻³) in GC12 is one of the major reasons causing an overestimate in nitrate and ammonium
30 mass concentrations compared to surface monitoring networks over the US. After replacing the



1 fixed value of in-cloud condensation water with MERRA-2 cloud and rain water, we get an
2 updated equation for rainout loss fraction (Luo et al., 2019):

3
$$F = \frac{f_c \cdot P_r}{k(LCW + P_r \cdot \Delta t)} (1 - e^{-k \cdot \Delta t}), \quad (1)$$

4 where F is the fraction of a water-soluble tracer in the grid-box scavenged by rainout, Δt (s) is
5 the model integration time step. k is the first-order rainout loss rate which represents the
6 conversion of cloud water to precipitation water. f_c , P_r ($\text{g} \cdot \text{m}^{-3} \cdot \text{s}^{-1}$), and LCW ($\text{g} \cdot \text{m}^{-3}$) are the grid-
7 box mean cloud fraction, the rate of new precipitation formation, and liquid phase cloud water
8 content, respectively.

9 L2019 also showed that the difference between observations and simulations can be
10 further reduced, through (1) the update of empirical washout coefficients by rain for water-
11 soluble aerosol with the value which was calculated by the parameterization of Laakso et al.
12 (2003) for a 500 nm particle diameter, and (2) the new estimated washout coefficients for nitric
13 acid by referring to field measurements for particles with a 10 nm diameter (Laakso et al., 2003)
14 and the theoretical dependence of scavenging coefficients on particle sizes for particles < 10 nm
15 (Henzing et al., 2006). L2019 only focused on warm cloud wet scavenging, and did not
16 systematically consider the impact of wet process treatments on the simulated aerosol precursors
17 and aerosols. Here we show that a number of treatments in GC12 and L2019 can be further
18 updated (as detailed below) to improve the performance of GEOS-Chem in simulating spatial
19 and temporal variations of major aerosol precursors and aerosols in a global scale.

20

21 **2.1 pH for cloud, rain, and wet surface**

22 Water pH is important for dissolution and subsequent aqueous phase reactions of water-
23 soluble gases (Turnock et al., 2019; Ervens, 2015; Pandis and Seinfeld, 1989). Based on Henry's
24 law, dissolution of water-soluble gases can be calculated as:

25
$$f_w = 1 - \frac{1}{1 + H^* \cdot R \cdot T \cdot LW}, \quad (2)$$

26 where f_w is the dissolution fraction for water-soluble gases, H^* ($\text{mol} \cdot \text{L}^{-1} \cdot \text{atm}^{-1}$) is effective
27 Henry's law constant, R ($0.08205 \text{ L} \cdot \text{atm} \cdot \text{K}^{-1} \cdot \text{mol}^{-1}$) is the gas constant, T (K) is the temperature,
28 and LW ($\text{m}^3 \cdot \text{m}^{-3}$) is the liquid water content.



1 H^* represents the impact of temperature, water acidity, and aqueous phase equilibrium on
 2 solubility of water-soluble species (Seinfeld and Pandis, 2016). For SO_2 , H_2O_2 , and NH_3 , which
 3 are important for aerosol precursor and aerosol simulation, can be calculated as (Seinfeld and
 4 Pandis, 2016):

$$\left. \begin{aligned} H_{\text{SO}_2}^* &= H_{\text{SO}_2} \left(1 + \frac{K_1}{[\text{H}^+]} + \frac{K_1 \cdot K_2}{[\text{H}^+]^2} \right), \\ H_{\text{SO}_2} &= 1.22 e^{10.55 \left(\frac{298.15}{T} - 1 \right)}, \\ K_1 &= 1.3 \times 10^{-2} e^{6.75 \left(\frac{298.15}{T} - 1 \right)}, \\ K_2 &= 6.31 \times 10^{-8} e^{5.05 \left(\frac{298.15}{T} - 1 \right)} \end{aligned} \right\} (3)$$

$$\left. \begin{aligned} H_{\text{H}_2\text{O}_2}^* &= H_{\text{H}_2\text{O}_2} \left(1 + \frac{K_3}{[\text{H}^+]} \right), \\ H_{\text{H}_2\text{O}_2} &= 8.3 \times 10^4 e^{24.82 \left(\frac{298.15}{T} - 1 \right)}, \\ K_3 &= 2.2 \times 10^{-12} e^{12.52 \left(\frac{298.15}{T} - 1 \right)} \end{aligned} \right\} (4)$$

$$\left. \begin{aligned} H_{\text{NH}_3}^* &= H_{\text{NH}_3} \left(1 + \frac{K_5 [\text{H}^+]}{K_4} \right), \\ H_{\text{NH}_3} &= 59.8 e^{14.1 \left(\frac{298.15}{T} - 1 \right)}, \\ K_4 &= 1. \times 10^{-14} e^{-22.5 \left(\frac{298.15}{T} - 1 \right)}, \\ K_5 &= 1.7 \times 10^{-5} e^{-14.5 \left(\frac{298.15}{T} - 1 \right)} \end{aligned} \right\} (5)$$

8 where H_{SO_2} , $H_{\text{H}_2\text{O}_2}$, and H_{NH_3} are the Henry's law constants for SO_2 , H_2O_2 , and NH_3 , respectively.
 9 K_1 , K_2 , K_3 , K_4 , and K_5 are rate coefficients for SO_2 reaction, HSO_3^- reaction, H_2O_2 reaction, H_2O
 10 reaction, and NH_3 reaction, respectively. The values of the Henry's law constants and rate
 11 coefficients are the same as those used in GEOS-Chem aqueous phase chemistry. $[\text{H}^+]$ (M) is the
 12 hydrogen ion concentration in cloud/rain droplets and at wet surfaces, which is related to pH as:

$$13 \quad [\text{H}^+] = 10^{-\text{pH}}, \quad (6)$$

14 GC12 calculates cloud water pH iteratively by using the concentrations of sulfate, total
 15 ammonium (ammonium + ammonia), total nitrate (nitrate + nitric acid), SO_2 , and CO_2 based on
 16 their effective Henry's law coefficients and cloud liquid water content in corresponding grid box



1 (Alexander et al., 2012). This iterative calculation is updated to use Newton's method in order to
2 arrive at a consistent result (Moch et al., 2019). To represent the removing of aerosols due to
3 rainout, GC12 assumes 30 % of sulfate, nitrate, and ammonium are removed away from cloud
4 water before cloud water pH calculation. To take into account the variations in the amount of
5 these species rained out, we propose to directly use the real-time rainout fractions for
6 corresponding species which are calculated during the treatment of wet scavenging to replace
7 this constant value (i.e., 30%). Additionally, in GC12, sulfate is assumed to be the only soluble
8 nonvolatile ion (SNVI) in cloud water, while ammonium and nitrate are treated as volatile
9 species similar to ammonia and nitric acid:

10
$$[\text{SNVI}] = 2[\text{SO}_4^{2-}], \quad (7)$$

11 Previous studies found that observed ammonium-sulfate aerosol molar ratio is lower than
12 2 over the US (Silvern et al., 2017; Hidy et al., 2014). Guo et al. (2018) found ammonium-sulfate
13 aerosol molar ratio during the Wintertime Investigation of Transport, Emissions, and Reactivity
14 (WINTER) study to be 1.47 ± 0.43 and pointed out that this phenomena indicates an important
15 role of soluble nonvolatile cations in aerosol thermodynamics. To reflect the impact of soluble
16 nonvolatile cations on cloud water pH, we assume that total amount of soluble nonvolatile
17 cations associated with aerosol thermodynamics (SNVC) is 25 % of sulfate. We also consider the
18 contribution of calcium and magnesium based on simulated dust mass in GC12, assuming that 3%
19 of dust mass is soluble calcium and 0.6% is soluble magnesium, (Farlie et al., 2010; Moch et al.,
20 2019) to soluble nonvolatile ions (SNVI):

21
$$[\text{SNVI}] = 2[\text{SO}_4^{2-}] - 2[\text{SNVC}] - 2[\text{Ca}^{2+}] - 2[\text{Mg}^{2+}], \quad (8)$$

22 Rainwater pH, which is used for the calculation of water-soluble gases' effective Henry's
23 law constants for rain droplets (Eqs. 3-5), is assumed to be a constant value of 4.5 in GC12.
24 Rainwater pH is determined by the cloud water pH where the rain is produced, uptakes of water
25 and ions during rainfall processes, and evaporation of rain droplets. In addition, rainwater pH
26 also depends on temperature (Smith and Martell, 1976). Although it is difficult to fully trace
27 rainwater pH in the model based on current available information in GC12, we use cloud pH at
28 where rainout occurs to represent rainwater pH for rainout process and rainwater-mass-weighted
29 cloud pH above where washout occurs to represent rainfall water pH for washout process in this
30 work.



1 pH values also affect dry deposition of water-soluble gases at wet surface via its impact
2 on the uptakes due to dissolution, therefore the origin of surface water is important. GC12
3 calculated effective Henry's constant for dry deposition by assuming temperature of 298.15 K
4 and leaf water pH of 7. Surface water of land is dominated by leaf water whose pH is ~7. pH of
5 ocean surface water varies from 8 to 8.5 (Antonov, 2010; Jacobson, 2005). de Caritat et al. (2005)
6 found the pH of the meltwaters of the Arctic snow varies from 4.6 to 6.1 with median value of
7 5.4. So we assume the pH values at wet surface are 7 for land, 8.2 for ocean, and 5.4 for snow in
8 this work.

9

10 **2.2 Fraction of cloud available for aqueous phase chemistry**

11 In GC12, the fraction of cloud available for aqueous phase chemistry is assumed to be
12 100 % of grid box cloud fraction when temperatures are above 258 K and 0 % of grid box cloud
13 fraction when temperatures are below 258 K. It means aqueous phase chemistry in mixed cloud
14 where temperatures are often below 258 K is not considered in GC12. However, many studies
15 indicated that supercooled cloud water can exist when temperatures are above 237 K (Rosenfeld
16 and Woodley, 2000; Sassen, 1985). Therefore, we propose to calculate aqueous phase cloud
17 fraction based on MERRA-2 cloud liquid content and cloud ice content when temperatures are
18 higher than 237 K and lower than 263 K:

$$19 \quad f_{aq} = f_c \frac{LCW}{LCW+ICW}, \quad (237 \text{ K} < T < 263 \text{ K}), \quad (9)$$

20 where f_{aq} is aqueous phase cloud fraction, LWC (g m^{-3}) is grid box mean liquid phase cloud
21 water content, and ICW (g m^{-3}) is grid box mean ice phase cloud water content.

22 The surface pre-melt layer or quasi-liquid layer occurs when temperatures are above 263
23 K (Nenow, 1984; Ocampo and Klinger, 1983). Conklin et al. (1993) suggested that the ice
24 surface can be modeled as an aqueous phase when temperatures are higher than 265 K. So for
25 temperature higher than 263 K, we assume aqueous phase cloud fraction equals grid mean cloud
26 fraction:

$$27 \quad f_{aq} = f_c, \quad (T > 263 \text{ K}), \quad (10)$$

28 The 263 K cut-off used here is to reflect the cover of meltwater on ice when temperature
29 is not too low.

30



1 2.3 Rainout efficiencies

2 2.3.1 Warm cloud

3 GEOS-Chem used rainout efficiencies to represent the absorptions of water-soluble
4 gasses and aerosols in the cloud condensate phase (Jacob et al., 2000; Mari et al., 2000; Liu et al.,
5 2001). After applying them with the updated parameterization for rainout loss fraction (Luo et al.,
6 2019), we get the new equation as

$$7 \quad F = \frac{f_c \cdot P_r}{k(LCW + P_r \cdot \Delta t)} (1 - e^{-E_r \cdot k \cdot \Delta t}), \quad (11)$$

8 where E_r is the rainout efficiency for corresponding species. Eq. (11) is the same as Eq. (1)
9 except Eq. (11) contains E_r in the rainout calculation.

10 In GC12, rainout efficiencies for water-soluble aerosols are assumed to be 100 % while
11 those for water-soluble gases, except nitric acid and SO_2 , are calculated via Henry's law
12 constants (Jacob et al., 2000). E_r of nitric acid is assumed to be the same as water-soluble
13 aerosols due to its high solubility. Due to the low solubility of SO_2 in water, rainout of SO_2 is
14 limited by the aqueous phase oxidation of SO_2 by H_2O_2 rather than the absorption by cloud water
15 (Chin et al., 1996). E_r of SO_2 in GC12 is assumed to be the same as water-soluble aerosols but
16 limited by the availability of H_2O_2 in the precipitating grid box. However, GEOS-Chem already
17 accounted for in-cloud oxidation of SO_2 as part of the aqueous phase chemical calculation, so
18 doing the same in the scavenging calculation would be double-counting the removal of SO_2 .
19 Considering the low solubility of SO_2 in water, it is more appropriate to calculate rainout
20 efficiency for SO_2 based on Henry's law. In the present work, we assume E_r of SO_2 equals its
21 dissolution fraction:

$$22 \quad E_{r_SO_2} = f_{w_SO_2}, \quad (12)$$

23 with $f_{w_SO_2}$ calculated with Eq. (2).

24 In the present work, we also modified rainout efficiencies for hydrophilic black carbon
25 (BC) and primary organic carbon (POC), from 100% in GC12 to 50%. The rationale for the
26 modification is that, although the aging of BC and POC in the atmosphere converts these
27 aerosols from hydrophobic to hydrophilic, they are not as easy to be activated into cloud droplet
28 as water-soluble aerosols (sulfate, nitrate, ammonium and so on). The composition of the
29 particles decide the hygroscopic parameter kappa which is important for cloud activation
30 calculation. If BC and POC are internally mixed with the sulfate, nitrate, ammonium (SNA)



1 aerosols, then they all have similar compositions. However, in the actual atmosphere, many
2 particles are externally mixed: some particles are pure SNA while others are primary particles
3 (BC, POC, dust, etc.) coated with SNA. It takes time for primary particles to gain coating
4 through condensation, coagulation, and aqueous chemistry. The amount of SNA coated on
5 primary particles depends on the aging time and abundance of SNA in the air. Based on detailed
6 size and mixing state resolved advanced particle microphysics (APM) simulation which
7 explicitly resolves the amount of SNA coating (Yu et al., 2012), the hygroscopic parameter
8 kappa of coated BC and POC is roughly about half of that of SNA. More robust calculation of
9 rainout efficiencies for BC and POC shall consider the amount of soluble species coated on these
10 particles (Yu et al., 2012; Yu and Luo, 2009) but this will be the subject of future work.

11

12 **2.3.2 Mixed and cold clouds**

13 In GC12, aerosols in mixed cloud ($237 \text{ K} \leq T < 258 \text{ K}$) and cold cloud ($T < 237 \text{ K}$) were
14 assumed to be removed through heterogeneous and homogeneous freezing nucleation (Wang et
15 al., 2014). GEOS-Chem assumed that heterogeneous nucleation dominates ice formation at
16 $237 \text{ K} \leq T < 258 \text{ K}$ (mixed cloud) and results in 100 % rainout efficiencies only for dust and
17 hydrophobic black carbon which are considered as ice nuclei (IN). Homogeneous nucleation
18 takes place at $T < 237 \text{ K}$ (cold cloud) and results in 100 % rainout efficiencies for both water-
19 soluble aerosol and IN.

20 Ice nucleation processes and their impacts on aerosol wet scavenging by mixed and cold
21 cloud are largely unclear. However, it is known that ice nucleation rates depend strongly on
22 temperature (DeMott et al., 2015; Kanji and Abbatt, 2010). To take into account this, we propose
23 to parameterize rainout efficiencies at warmer temperature based on the fraction of dust in mixed
24 cloud contributing to IN, which can be calculated as a function of T according to DeMott et al.
25 (2015) as:

$$26 \quad E_{r_mixed_dust} = \frac{e^{0.46(273.16-T)-11.6}}{153.5}, \quad (237 \text{ K} \leq T < 258 \text{ K}), \quad (13)$$

27 In addition to T, ice nucleation efficiency of particles also depend on their sizes and
28 smaller particles (diameter $< 500 \text{ nm}$) are less likely to act as IN (Niedermeier et al., 2015).
29 While most of mass of dust particles are dominated by those larger than 500 nm, a significant
30 fraction of BC particles are smaller than 500 nm. Based on sectional aerosol microphysics



1 calculation in GEOS-Chem-APM (Yu and Luo, 2009), the mass fraction of BC particles with
2 diameter > 500 nm is ~ 50 %. In this study, we assume E_r for hydrophobic BC in both mixed
3 cloud ($237 \text{ K} \leq T < 258 \text{ K}$) and cold cloud ($T < 237 \text{ K}$) are 50 % of those values for dust.

4 Water-soluble aerosols are removed via homogeneous freezing nucleation in cold cloud
5 (Wang et al., 2014; Liu et al., 2001). Strom et al. (1997) observed that ~ 40 % of preexisting
6 aerosol mass is incorporated in ice crystal. In this work, we assume cold cloud rainout
7 efficiencies are 40 % for water-soluble aerosol, 50 % for hydrophobic black carbon, and 100 %
8 for dust, respectively.

9 In GC12, cold cloud wet scavenging of nitric acid is treated the same as water-soluble
10 aerosol. However, in cold cloud ($T < 237 \text{ K}$), nitric acid is removed by the partition on ice crystal
11 (Kärcher and Voigt, 2006; Voigt et al., 2006), while water-soluble aerosol is removed by
12 homogeneous freezing nucleation. Kärcher et al. (2008) used climatology of cirrus ice water
13 content together with observed molar ratios of $\text{HNO}_3/\text{H}_2\text{O}$ in cirrus ice particles to estimate the
14 range of nitric acid content in cirrus ice (185-240 K). Their study showed that less efficient nitric
15 acid uptake limits the nitric acid content in cirrus ice at higher temperatures and small ice water
16 contents permit only little nitric acid in ice at low temperatures. Fraction of nitric acid in ice
17 generally increases with decreasing temperature. Kärcher and Voigt (2006) attributed this
18 behavior to less efficient nitric acid trapping at higher temperatures despite faster ice growth
19 rates, which is caused by increasingly rapid escape of adsorbed nitric acid into the gas phase. A
20 parameterization of nitric acid partitioning in cold cloud developed by Kärcher et al. (2008) is
21 employed here to calculate E_r of nitric acid in cold cloud when temperature is below 240 K:

$$22 \quad E_r = \frac{10^{-(26.5 \times 1.00155^T + 30.7)} \cdot \frac{63}{18} \cdot \left[\frac{\text{LCW} + \text{ICW}}{f_c} \right]_{\text{vmr}}}{[\text{HNO}_3]_{\text{vmr}}}, \quad (14)$$

23 where $\left[\frac{\text{LCW} + \text{ICW}}{f_c} \right]_{\text{vmr}}$ is volume mixing ratio of in-cloud water and in-cloud ice, and
24 $[\text{HNO}_3]_{\text{vmr}}$ is volume mixing ration for nitric acid gas.

25

26 **2.4 In-cloud condensation water for cold cloud**

27 In GC12, ICCW for cold cloud ($T < 237 \text{ K}$) is assumed to have a fixed value of $1 \text{ g} \cdot \text{m}^{-3}$
28 which is the same as that of warm cloud. This assumption significantly underestimates wet



1 scavenging due to rainout in cold cloud ($T < 237$ K). L2019 replaced the fixed ICCW with cloud
2 water and rain water as shown in Equ. 1. However, water-soluble aerosols in cold cloud ($T < 237$
3 K) can also exist in ice due to freezing of supercooled water, therefore, we calculate ICCW for
4 cold cloud as:

$$5 \quad \text{ICCW}_c = \frac{\text{LCW} + \text{ICW} + P_r \cdot \Delta t}{f_c}, \quad (15)$$

6

7 **2.5 Empirical washout coefficients by rain and snow**

8 Washout coefficients by rain and snow in GC12 were updated by Wang et al. (2011) by
9 adopting the parameterization constructed by Feng (2007, 2009) for individual aerosol modes.
10 Accumulation-mode washout coefficients were used for all aerosols except dust and sea salt, for
11 which the coarse mode coefficients were used. Previous studies noticed that washout rates by
12 rain derived from field measurements are 1 to 2 orders of magnitude larger than the values from
13 theoretical calculation (Wang et al., 2010; Luo et al., 2019). Therefore, L2019 recommended
14 using empirical washout coefficients for the simulation of washout by rain.

15 Wang et al. (2014) found that the large differences in washout rate between field
16 measurements and theoretical calculation not only appear in washout by rain but also appear in
17 washout by snow. In this work, we use the semi-empirical parameterization developed by Wang
18 et al. (2014) for the calculation of nitric acid and aerosol washout by both rain and snow.
19 Washout rate is calculated by an exponential equation:

$$20 \quad k_{\text{wash}} = \Lambda \left(\frac{P_d}{f_r} \right)^b, \quad (16)$$

21 where k_{wash} (s^{-1}) is the washout rate, P_d (mm h^{-1}) is rain or snow falling from upper layers, f_r is
22 rainfall area fraction, Λ is washout scavenging coefficient, and b is an exponential coefficient.

23 The values of Λ and b for nitric acid and aerosol washout by rain ($T > 268$ K) and snow
24 ($248 \text{ K} < T < 268 \text{ K}$) are shown in Table 1. We assume precipitation at temperatures lower than
25 248 K is dominated by ice. GC12 assumed washout of aerosol by ice is the same as that by snow.
26 However, uptake of aerosol by ice and by snow are different. Schneider et al. (2019) found
27 specific surface area (SSA) of ice crystal is $\sim 1/5$ of SSA of snow. Therefore, in this work, we
28 roughly assume washout rate by ice ($T < 248$ K) is $1/5$ of that by snow. Washout of nitric acid
29 uses the same values in the work of Luo et al. (2019) but extend the temperature limitation from



1 268 K to 248 K. Washout of nitric acid by ice is assumed to be 1/5 of that by snow. Empirical
2 washout coefficients by rain and snow for coarse aerosol and hydrophobic fine aerosol in this
3 work are based on the values in Wang et al. (2014). Because the rain washout rate for water-
4 soluble aerosols measured by Laakso et al. (2003) is still ~ 20 times larger than that calculated by
5 the semi-empirical parameterization, we used the value of 1×10^{-5} to replace 5×10^{-7} for
6 hydrophilic aerosol's washout by rain. The washout coefficient of hydrophilic aerosol by snow is
7 replaced with the value of 2×10^{-4} which is 20 times higher than the value by rain. Washout by ice
8 is assumed to be 1/5 of that by snow.

9

10 **2.6 Wet surface uptakes during dry deposition**

11 Uptakes at wet surface are strongly influenced by dissolution processes. The solubility of
12 SO_2 , H_2O_2 , and NH_3 at wet surface needs to be calculated via effective Henry's law coefficient
13 because it is associated with a series of aqueous phase reactions (Seinfeld and Pandis, 2016). In
14 GC12, H^* of SO_2 , H_2O_2 , and NH_3 for dry deposition are assumed to be the constants with the
15 values of 10^5 M atm^{-1} , $5 \times 10^7 \text{ M atm}^{-1}$, and $2 \times 10^4 \text{ M atm}^{-1}$, respectively
16 ([http://wiki.seas.harvard.edu/geos-chem/index.php/Physical_properties_of_GEOS-
17 Chem_species#Definition_of_Henry.27s_law_constants](http://wiki.seas.harvard.edu/geos-chem/index.php/Physical_properties_of_GEOS-Chem_species#Definition_of_Henry.27s_law_constants)). In this work, we consider the impacts
18 of temperature and pH at wet surface on the values of H^* (Erisman et al., 1994; Wesely et al.,
19 1990), and the values of H^* for SO_2 , H_2O_2 , and NH_3 are calculated with equations (3-5). Wet
20 surface pHs discussed in section 2.1 are used to reflect the impact of wet surface acidity on
21 dissolution during dry deposition. Ganzeveld et al. (1998) reported that observations and
22 physical-chemical model simulations indicated SO_2 dry deposition velocity increases from a
23 minimum value of 0.01 cm s^{-1} for a temperature of 253 K to a value of $0.15\text{-}0.25 \text{ cm s}^{-1}$ for 273
24 K. Therefore, in this work, we assume SO_2 dry deposition velocity over snow and ice is 0.01 cm
25 s^{-1} when temperatures are lower than 253 K.

26

27 **3. Results and discussions**

28 To investigate the impacts of updated wet processes on global simulation of aerosol
29 precursors and aerosols, we run GEOS-Chem for 3 cases: (1) standard Geos-Chem version
30 12.6.0, called GC12; (2) the same as case GC12 except using wet scavenging described in the
31 work of Luo et al. (2019), and this case is named L2019; (3) the same as the case L2019 except



1 considering the updated wet processes described in section 2, and this case is called WETrev. All
2 simulations are run with $2^{\circ} \times 2.5^{\circ}$ horizontal resolution and 47 layers from surface to 0.01 hPa.
3 Emissions are produced by the default setting of HEMCO (Keller et al., 2014).

4

5 **3.1 Comparison with surface monitoring networks over the US, Europe, and East Asia**

6 Figure 1 and Table 2 present the comparisons of observed secondary inorganic aerosol
7 precursors and secondary inorganic aerosols at surface monitoring networks and the simulated
8 mass concentrations by the GC12, L2019, and WETrev cases described above. At the United
9 States, SO_2 , nitric acid, ammonia surface mass concentration measurements were collected from
10 USEPA, CASTNET, and AMoN, respectively. Measurements of secondary inorganic aerosols
11 were collected from IMPROVE and CSN. Surface mass concentrations of secondary inorganic
12 aerosol precursors and secondary inorganic aerosols over Europe and Asia were observed by
13 EMEP and EANET, respectively. As shown in Fig. 1 (a-c), simulated SO_2 for the 3 cases is
14 lower than observed values over the US but higher than the observations over Europe and Asia.
15 Over the US, simulated SO_2 is $\sim 20\%$ lower than observations. One possible reason is that a
16 large amount of USEPA observations are located at urban regions where SO_2 concentrations are
17 much higher than rural and remote regions. After considering the updates of wet scavenging by
18 L2019, NMBs are reduced from 101 % to 84 % over Europe and from 63 % to 43 % over Asia,
19 respectively. Considering of updated wet processes in this work further reduces NMBs to 73 %
20 at Europe and 23 % at Asia, respectively.

21 Figure 1 (d-f) are the results for nitric acid. NMBs of simulated nitric acid by GC12 for
22 the US, Europe, and Asia are 89 %, 44 %, and 136 %, respectively. G12 simulation significantly
23 overestimates surface mass concentration of nitric acid at these regions. Simulations by L2019
24 and WETrev indicate that wet scavenging is the dominant process causing the overestimation of
25 nitric acid in GEOS-Chem. NMBs of simulated nitric acid in WETrev for the US, Europe, and
26 Asia are reduced to 13 %, -20 %, -18 %, respectively. We also notice that WETrev
27 underestimates nitric acid at low temperatures for US and Europe sites. These underestimates
28 may be associated with the updated uptake coefficients by Holmes et al. (2019) for
29 heterogeneous chemistry. If we switch back to the old heterogeneous chemistry in GEOS-Chem
30 version 12.5, the underestimation of nitric acid at low temperatures is reduced (not shown).
31 Figure 1 (g-i) show the biases of model simulated ammonia by the 3 cases over the 3 regions are



1 small. The aqueous concentration of ammonia is much lower than nitric acid, and therefore wet
2 processes show relatively small impact on the simulation of ammonia.

3 Figure 1 (j-l) are observed and simulated sulfate at the US, Europe, and Asia. NMBs of
4 the GC12 case over the 3 regions are -1.1 %, 27 %, and 5.5 %, respectively. The application of
5 updates of wet scavenging in L2019 leads to significantly underestimation of sulfate during
6 winter time, reaching up to 50 % over the 3 regions. Based on our investigation, we found that
7 the missing of aqueous phase chemistry in mixed cloud appears to be the main reason of
8 underestimated sulfate at low temperatures. As we discussed in section 2, aqueous phase
9 chemistry in GC12 is only simulated when temperatures are higher than 258 K. Conversely, in
10 WETrev case, the temperature limitation of aqueous phase chemistry is extended from 258 K to
11 237 K. This change allows aqueous phase chemistry to be simulated when temperatures are low.
12 After employing the new approaches of cloud water pH and aqueous phase cloud fraction
13 calculation, NMBs of the WETrev case at the 3 regions are -11 %, 15 %, and -7.0 %,
14 respectively. It significantly reduces the bias shown in the L2019 case. The absence of aqueous
15 phase hydroxymethanesulfonate chemistry may be a potential reason for the remaining model
16 biases with sulfate, but this is not explored here (Moch et al., 2018). As shown in Figure 1 (m-r),
17 simulated nitrate and ammonium by GC12 case over the 3 regions are much higher than
18 observations. As discussed in Luo et al. (2019), the overestimation is associated with the
19 underestimation of rainout and washout of nitric acid and nitrate. Updated wet scavenging in
20 L2019 successfully reduces NMBs of nitrate over the 3 regions from 126 % to 10 %, 105 % to --
21 14 %, and 269 % to 47 %, respectively. NMBs of ammonium over the 3 regions are reduced
22 from 45 % to -13 %, 91 % to -3.3 %, and 167 % to 42 %, respectively. Updated wet processes in
23 this work show relatively small impact on simulated nitrate and ammonium surface mass
24 concentrations over the 3 regions.

25 Figure 2 is the comparison of observed BC and OC over the US and Europe. Simulated
26 BC over the US is close to the observations except for a 10-20 % underestimate during summer
27 and fall. The underestimate is likely associated with the underestimated wildfire emissions in the
28 western US. Simulated OC over the US is close to the observations during summer but 50-60 %
29 lower than observations during spring and fall. GEOS-Chem (all three cases) significantly
30 underestimated BC and OC over Europe and the possible reasons behind the bias remain to be
31 investigated. NMBs of the 2 species in Europe are high up to -37 % and -61 %, respectively. The



1 differences of simulated BC and OC in the 3 cases are small for the US and Europe which
2 indicates wet processes have a small impact on the simulation of BC and OC in these regions.
3 The small impact of wet processes on BC in the US and Europe is because 80 % of emitted BC is
4 assumed to be hydrophobic aerosol which needs 1.15 days to be converted to hydrophilic BC.
5 Updated wet processes has little impact on hydrophobic aerosol in low troposphere where wet
6 scavenging is dominated by warm cloud. OC consists of primary organic aerosol (POA) and
7 SOA which is formed through the oxidation of organic gaseous precursors. Due to low solution
8 of POA and organic gaseous precursors in water, wet processes can have little impact on these
9 species.

10

11 **3.2 Comparison of SO₂, sulfate and BC mass concentrations at Arctic sites**

12 We also studied the impact of updated wet processes on SO₂, sulfate and BC surface
13 mass concentrations at several Arctic sites where measurements are available. Figure 3 shows the
14 comparison of SO₂ at Nord (81.6°N, 16.7°W) and Zeppelin (78.9°N, 11.9°E). GC12 case matches
15 well with the observed SO₂ at Nord but 3 times overestimated SO₂ at Zeppelin in January and
16 December. The updated wet scavenging (yellow line) shows small impact on SO₂ simulation at
17 Arctic. Simulated SO₂ is slightly reduced during winter and spring. In WETrev case, we assumed
18 SO₂ dry deposition velocity is 0.01 cm s⁻¹ when temperatures are lower than 253 K. It slightly
19 enhances SO₂ at the higher latitude site Nord during winter. Figure 4 is the observed and
20 simulated sulfate and BC at Alert (82.5°N, 62.5°W), Barrow (71.3°N, 156.6°W), and Zeppelin.
21 Observations at the 3 sites show that both sulfate and BC are high in spring and low in summer.
22 Model simulation generally captures seasonal variation at these Arctic sites. However, GC12
23 overestimates sulfate mass concentration at the 3 sites by a factor of 2-3. Simulated BC by GC12
24 is 50 % lower than observation at Alert during spring and a factor of 2 higher than observations
25 at Barrow and Zeppelin during winter. Updated wet scavenging significantly impacts simulated
26 sulfate and BC in Arctic regions. Simulated sulfate by L2019 is much closer to observations
27 except for a 50 % underestimation at Alert during spring, while simulated BCs at the 3 Arctic
28 sites by L2019 is much lower than observations. The comparison with model results from
29 WETrev shows the underestimation of sulfate at Alert during spring is compensated by
30 considering aqueous phase chemistry in mixed clouds. Most of BC at Arctic regions is
31 transported from middle-low latitude source regions with open fire and anthropogenic emissions,



1 and during the long-range transport hydrophobic BC is aged and covered to hydrophilic BC. The
2 assumption of reduced hydrophilic BC rainout efficiency in the WETrev case increases
3 simulated BC mass concentration and enhances agreement with observations at these Arctic sites.

4

5 **3.3 Vertical profiles of nitric acid and aerosols: Comparison with ATom-1 and ATom-2** 6 **aircraft measurements**

7 To evaluate the impact of updated wet processes on simulated vertical profiles of aerosol
8 precursors and aerosols, we compare simulated nitric acid and aerosols for the 3 cases with the
9 aircraft measurements during ATom-1 in July-August 2016 and ATom-2 in January-February
10 2017 over the North Hemisphere (Fig. 5) and the South Hemisphere (Fig. 6). Flight tracks over
11 the land or in the stratosphere are filtered out for the comparison.

12 As shown in Figure 5, GC12 overestimates nitric acid and underestimates black carbon
13 and organic carbon over the North Hemisphere during both ATom-1 and ATom-2. GC12
14 simulated sulfate and ammonium match well with observations during ATom-1 but are much
15 higher than observations during ATom-2. After considering the updated wet scavenging in Luo
16 et al. (2019), the overestimations of nitric acid, sulfate, and ammonium during ATom-2 and
17 nitric acid during ATom-1 are reduced. However, L2019 significantly underestimates nitric acid
18 at the upper troposphere where pressure is lower than 300 hPa. As we mentioned earlier, L2019
19 may overestimate cold cloud wet scavenging of nitric acid due to the old treatments in GC12.
20 With updated cold cloud scavenging in WETrev, bias of nitric acid simulated by L2019 at the
21 upper troposphere is reduced. Figure 5 (g) shows the impact of updated aqueous phase chemistry
22 in mixed cloud on the sulfate vertical profile. Considering aqueous phase chemistry in mixed
23 cloud significantly enhances sulfate mass concentration within the range of 700-500 hPa during
24 ATom-2 which makes the simulated sulfate much closer to observed values. Figures 5 (d) and (i)
25 indicate that the impact of updated wet scavenging on black carbon vertical profile during
26 ATom-2 is more obvious than that during ATom-1. It is because black carbon emitted from open
27 fire in January is much less than that in July. Black carbon observed during ATom-2 is
28 dominated by hydrophilic black carbon which is more affected by wet scavenging processes,
29 while black carbon observed during ATom-1 is dominated by hydrophobic black carbon.
30 Updated wet scavenging shows small impact on organic carbon vertical profiles during both
31 ATom-1 and ATom-2.



1 Figure 6 shows the comparisons over the South Hemisphere. Updated wet scavenging
2 reduces overestimated nitric acid especially during ATom-1 period. For sulfate, ammonium,
3 black carbon, and organic carbon, the differences among the 3 cases are relative small. All cases
4 significantly underestimate black carbon from open fire and upper troposphere organic carbon.
5 Based on the comparisons with ATom-1 and ATom-2 measurements, it is clear that the updated
6 wet process treatments in this work can improve the agreements of simulated and observed
7 vertical profiles of nitric acid and aerosols.

8

9 **3.4 Impact on global distributions of surface mass concentrations**

10 The impacts of updated wet process treatments on global simulation of surface mass
11 concentrations are shown in Figures 7-11. Figures 7-9 are simulated surface mass concentrations
12 of secondary inorganic aerosol precursors (SO₂, nitric acid, and ammonia), secondary inorganic
13 aerosols (sulfate, nitrate, and ammonium), primary inorganic aerosols (sea-salt, dust, and black
14 carbon), and organic carbon (primary organic aerosol and secondary organic aerosol) simulated
15 by GC12 case and WETrev case, while figures 10-11 are the percentage differences.

16 As shown in Figure 7, high values of secondary inorganic aerosol precursors are mainly
17 located at continental regions with high anthropogenic and natural emissions. After considering
18 the updated wet process treatments in this study, global mean surface mass concentrations
19 (GMSMC) of SO₂, nitric acid, and ammonia are changed from 0.76 μg m⁻³, 0.55 μg m⁻³, 0.32 μg
20 m⁻³ to 0.78 μg m⁻³, 0.28 μg m⁻³, 0.43 μg m⁻³, respectively. The updated wet process treatments
21 slightly impact GMSMC of SO₂ but strongly impact GMSMC of nitric acid. The impact on
22 ammonia is small over land but strong over ocean. The weak impact of the updated wet process
23 treatments on SO₂ is because its wet removal is dominated by aqueous phase chemistry. The
24 strong impact of the updated wet process treatments on ammonia over ocean is due to the
25 changes of rainwater pHs over remote regions whose values are higher than the assumed 4.5
26 rainwater pH in GC12. Some large changes of surface mass concentration at Arctic and Antarctic
27 regions, as shown in Figure 10 (a-c), are associated with the updated treatments of wet surface
28 uptakes during dry deposition at snow and ice. However, due to low mass concentrations at
29 Arctic and Antarctic regions, their impacts on GMSMC are small. The updated wet process
30 treatments exhibit significant impact on GMSMC of secondary inorganic aerosols whose water
31 solubility is high. After considering the updated wet process treatments, GMSMC of sulfate,



1 nitrate, and ammonium are changed from $0.87 \mu\text{g m}^{-3}$, $0.41 \mu\text{g m}^{-3}$, $0.34 \mu\text{g m}^{-3}$ to $0.76 \mu\text{g m}^{-3}$,
2 $0.22 \mu\text{g m}^{-3}$, $0.27 \mu\text{g m}^{-3}$, respectively. Their global mean relative changes are high up to -25 %, -
3 51 %, and -22 %, respectively. Most of the reductions of these species happen at middle-high
4 latitude regions with high mass concentrations.

5 Figures 9 and 11 show the impacts of updated wet process treatments on primary
6 inorganic aerosols and organic carbon. It is clear that the updated wet process treatments have
7 little impact on GSMSCs of these species. For sea salt, its high concentrations are mainly
8 located at middle latitude regions in both the North Hemisphere and South Hemisphere where in
9 cloud condensation water values are close to the assumed constant value in GC12. Therefore, the
10 differences of wet scavenging in GC12 and WETrev cases at these regions are small. For dust,
11 due to its low water solubility, the updated wet processes show small impact in the lower
12 troposphere where wet scavenging is dominated by warm cloud. Most of black carbon and
13 organic carbon are emitted as hydrophobic aerosols and then converted to be hydrophilic
14 aerosols due to aging. Therefore, the updated wet process treatments show small impact at source
15 regions but strong impact at remote regions.

16

17 **4. Summary**

18 In this study, we updated aqueous phase chemistry and wet scavenging for SO_2 and
19 sulfate, rainout efficiencies for warm, mixed, and cold cloud, empirical washout by rain and
20 snow, and wet surface uptakes during dry deposition in GEOS-Chem version 12.6.0 and
21 presented the validations of simulated aerosol precursors and aerosols with ground based
22 monitoring networks over the US, Europe, and Asia, in-site observations at Arctic for surface
23 mass concentrations and aircraft measurements during ATom-1 and ATom2 for their vertical
24 profiles. Based on these validations, we found:

- 25 (1) The model results with the updated treatment of wet processes agree better with
26 measurements for most species in different regions, especially for nitric acid, nitrate,
27 and ammonium;
- 28 (2) The updated aqueous phase chemistry and wet scavenging of SO_2 and sulfate
29 significantly improve the agreement of simulated SO_2 and sulfate at the US, Europe,
30 and Asia, especially during the winter time;



- 1 (3) The updated rainout efficiencies enhance BC mass concentration at remote regions
2 and successfully reduce the bias between simulation and observation at Arctic sites;
3 (4) Cold cloud scavenging plays an important roles in the simulation at the upper
4 troposphere, especially for nitric acid;
5 (5) The updated wet surface uptake during dry deposition improves the agreement of
6 simulated SO₂ at Arctic sites.

7 Wet processes are important for atmospheric chemistry modeling. Our study indicates
8 that the updated wet process treatments introduced in this study have strong impacts on global
9 means of water soluble aerosol precursors and aerosols such as nitric acid, sulfate, nitrate, and
10 ammonium. The updated wet process treatments exhibit relatively small impacts on the
11 simulated global means of SO₂, dust, sea salt, black carbon, and organic carbon. Although we
12 tried to make the updated wet process treatments to be the state-of-the-art, there still exit
13 limitations of the work presented in this study. For example, washout efficiencies of water
14 soluble species such as SO₂ and ammonia are sensitive to rain water pH values. In this study, we
15 simply assumed rainwater pHs for rainout and washout are cloud pH at where rainout occurs and
16 rainwater-mass-weighted cloud pH above where washout occurs, respectively. However, rain
17 water pH needs to be calculated by tracing the cloud process and precipitation process of rain
18 water lifecycle. The impact of traced rain water pH on wet scavenging needs to be further
19 investigated.

20
21 Code and data availability. The code of GEOS-Chem 12.6.0 is available through the GEOS-
22 Chem distribution web-page http://wiki.seas.harvard.edu/geos-chem/index.php/GEOS-Chem_12.
23 All measurement data are publicly available.

24

25 Author contributions. GL and FY proposed and implemented the improved wet processes
26 schemes and validated model simulations with surface observations and ATom aircraft
27 measurements. MJ provided the new cloud pH approach in GEOS-Chem. All authors contributed
28 to the writing and editing of the paper.

29



1 Competing interests. The authors declare that they have no conflict of interest.

2

3 Acknowledgments. This work is supported by NYSERDA under contract 137487, NASA under
4 grant NNX17AG35G, and NSF under grant 1550816. The authors thank Daniel J. Jacob,
5 Harvard University, whose comments and suggestions greatly helped improve and clarify this
6 paper. We would like to acknowledge the United States Environmental Protection Agency
7 (USEPA), the Interagency Monitoring of Protected Visual Environments (IMPROVE), the
8 Chemical Speciation Network (CSN), the Clean Air Status and Trends Network (CASTNET),
9 the Ammonia Monitoring Network (AMoN), the European Monitoring and Evaluation
10 Programme (EMEP), and the Acid Deposition Monitoring Network in East Asia (EANET) for
11 the in-site measurement data. We would like to acknowledge the Atmospheric Tomography
12 Mission (ATom) for the aircraft measurement data. GEOS-Chem is a community model
13 maintained by the GEOS-Chem Support Team at Harvard University.

14

15 References

- 16 Alexander, B., D.J. Allman, H.M. Amos, T.D. Fairlie, J. Dachs, D.A. Hegg and R.S. Sletten,
17 Isotopic constraints on sulfate aerosol formation pathways in the marine boundary layer
18 of the subtropical northeast Atlantic Ocean, *J. Geophys. Res.*, 117, D06304,
19 doi:10.1029/2011JD016773, 2012.
- 20 Amos, H. M., Jacob, D. J., Holmes, C. D., Fisher, J. A., Wang, Q., Yantosca, R. M., Corbitt, E. S.,
21 Galarneau, E., Rutter, A. P., Gustin, M. S., Steffen, A., Schauer, J. J., Graydon, J. A.,
22 Louis, V. L. St., Talbot, R. W., Edgerton, E. S., Zhang, Y., and Sunderland, E. M.: Gas-
23 particle partitioning of atmospheric Hg(II) and its effect on global mercury deposition,
24 *Atmos. Chem. Phys.*, 12, 591–603, <https://doi.org/10.5194/acp-12-591-2012>, 2012.
- 25 Antonov JI, Seidov D, Boyer TP, Locarnini RA, Mishonov AV, Garcia HE, Baranova OK,
26 Zweng MM, Johnson DR: World Ocean Atlas 2009, Volume 2: Salinity. In: Levitus S
27 (ed) NOAA Atlas NESDIS 69, US Government Printing Office, Washington, 2010.
- 28 Bey, I., Jacob, D. J., Yantosca, R. M., Logan, J. A., Field, B. D., Fiore, A. M., Li, Q., Liu, H. Y.,
29 Mickley, L. J., and Schultz, M. G.: Global modeling of tropospheric chemistry with



- 1 assimilated meteorology: Model description and evaluation, *J. Geophys. Res.*, 106(D19),
2 23073– 23095, doi:10.1029/2001JD000807, 2001.
- 3
- 4 Chin, M., Jacob, D. J., Gardner, G. M., Foreman - Fowler, M. S., Spiro, P. A., and Savoie, D. L.:
5 A global three - dimensional model of tropospheric sulfate, *J. Geophys. Res.*, 101(D13),
6 18667– 18690, doi:10.1029/96JD01221, 1996.
- 7 Chin, M., R. B. Rood, S.-J. Lin, J.-F. Muller, and A. M. Thompson: Atmospheric sulfur cycle
8 simulated in the global modelGOCART: Model description and global properties.*J.*
9 *Geophys.Res.*,105,24 671–24 687, 2000.
- 10 Conklin, M.H., Sommerfeld, R.A., Laird, K., Villinski, J.E.: Sulfur dioxide reactions on ice
11 surfaces: implications for dry deposition to snow. *Atmospheric Environment A* 27, 159-
12 167, 1993.
- 13 de Caritat, P., Hall, G., Gislason, S., Belsey, W., Braun, M.,Goloubeva, N. I., Olsen, H. K.,
14 Scheie, J. O., and Vaive, J. E.: Chemical composition of arctic snow: concentration level
15 andregional distribution of major elements, *Sci. Total Environ.*, 336,183–199, 2005.
- 16 DeMott, P. J., Prenni, A. J., McMeeking, G. R., Sullivan, R. C., Petters, M. D., Tobo, Y.,
17 Niemand, M., Möhler, O., Snider, J. R., Wang, Z., and Kreidenweis, S. M.: Integrating
18 laboratory and field data to quantify the immersion freezing ice nucleation activity of
19 mineral dust particles, *Atmos. Chem. Phys.*, 15, 393–409, [https://doi.org/10.5194/acp-15-](https://doi.org/10.5194/acp-15-393-2015)
20 393-2015, 2015.
- 21 Erisman, J. W., Van Pul, A., and Wyers, G. P.: Parameterizationof surface resistance for the
22 quantification of atmospheric deposition of acidifying pollutants and ozone, *Atmos.*
23 *Environ.*, 28,2595–2607, 1994.
- 24 Ervens, B., Turpin, B. J., and Weber, R. J.: Secondary organic aerosol formation in cloud
25 droplets and aqueous particles (aqSOA): a review of laboratory, field and model studies,
26 *Atmos. Chem. Phys.*, 11, 11069–11102, <https://doi.org/10.5194/acp-11-11069-2011>,
27 2011.
- 28 Fairlie, T. D., Jacob, D. J., Dibb, J. E., Alexander, B., Avery, M. A., van Donkelaar, A. and
29 Zhang, L.: Impact of mineral dust on nitrate, sulfate, and ozone in transpacific Asian
30 pollution plumes, *Atmos. Chem. Phys.*, 10(8), 3999–4012, doi:10.5194/acp-10-3999-
31 2010, 2010.



- 1 Feng, J.: A 3-mode parameterization of below-cloud scavenging of aerosols for use in
2 atmospheric dispersion models, *Atmos. Environ.*, 41, 6808–6822, 2007.
- 3 Feng, J.: A size-resolved model for below-cloud scavenging of aerosols by snowfall, *J. Geophys.*
4 *Res.-Atmos.*, 114, D08203, doi:10.1029/2008JD011012, 2009.
- 5 Ganzeveld, L., Lelieveld, J., and Roelofs, G. - J.: A dry deposition parameterization for sulfur
6 oxides in a chemistry and general circulation model, *J. Geophys. Res.*, 103(D5), 5679–
7 5694, doi:10.1029/97JD03077, 1998.
- 8 Garland, J.A. and Branson, J.R.: The deposition of sulphur dioxide to pine forest assessed by a
9 radioactive tracer method. *Tellus*, 29: 445-454. doi:10.1111/j.2153-3490.1977.tb00755.x,
10 1977.
- 11 Guo, H., Nenes, A., and Weber, R. J.: The underappreciated role of nonvolatile cations in aerosol
12 ammonium-sulfate molar ratios, *Atmos. Chem. Phys.*, 18, 17307–17323,
13 <https://doi.org/10.5194/acp-18-17307-2018>, 2018.
- 14 Henzing, J. S., Olivieri, D. J. L., and van Velthoven, P. F. J.: A parameterization of size resolved
15 below cloud scavenging of aerosols by rain, *Atmos. Chem. Phys.*, 6, 3363–
16 3375, <https://doi.org/10.5194/acp-6-3363-2006>, 2006.
- 17 Hidy, G. M., Blanchard, C. L., Baumann, K., Edgerton, E., Tanenbaum, S., Shaw, S., Knipping,
18 E., Tombach, I., Jansen, J., and Walters, J.: Chemical climatology of the southeastern
19 United States, 1999–2013, *Atmos. Chem. Phys.*, 14, 11893–11914,
20 <https://doi.org/10.5194/acp-14-11893-2014>, 2014.
- 21 Holmes, C. D., Bertram, T. H., Confer, K. L., Graham, K. A., Ronan, A. C., Wirks, C. K., &
22 Shah, V.: The role of clouds in the tropospheric NO_x cycle: A new modeling approach
23 for cloud chemistry and its global implications. *Geophysical Research Letters*, 46, 4980–
24 4990. <https://doi.org/10.1029/2019GL081990>, 2019.
- 25 Hopke, P.K., Ito, K., Mar, T., Christensen, W.F., Eatough, D.J., Henry, R.C., Kim, E., Laden, F.,
26 Lall, R., Larson, T.V., Liu, H., Neas, L., Pinto, J., Stöölzel, M., Suh, H., Paatero, P.,
27 Thurston, G.D.: PM source apportionment and health effects: 1. Intercomparison of
28 source apportionment results. *J. Expo. Sci. Environ. Epidemiol.* 16, 275e286, 2006.
- 29 Jacob, D. J., Liu, H., Mari, C., and Yantosca, B. M., Harvard wet de-position scheme for GMI,
30 available at:



- 1 http://acmg.seas.harvard.edu/geos/wiki_docs/deposition/wetdep.jacob_et_al_2000.pdf (last
2 access: December 2019), 2000.
- 3 Jacobson, M. Z.: Studying ocean acidification with conservative, stable numerical schemes for
4 nonequilibrium air - ocean exchange and ocean equilibrium chemistry, *J. Geophys. Res.*,
5 110, D07302, doi:10.1029/2004JD005220, 2005.
- 6 Kanji, Z. A., and J. P. D. Abbatt: Ice nucleation onto Arizona test dust at cirrustemperatures:
7 Effect of temperature and aerosol size on onsetrelative humidity.*J. Phys. Chem.*,114A,
8 935–941, 2010.
- 9 Kärcher, B., and Voigt, C.: Formation of nitric acid/water ice particles in cirrus clouds, *Geophys.*
10 *Res. Lett.*, 33, L08806, doi:10.1029/2006GL025927, 2006.
- 11 Kärcher, B., M., C. Schiller, C. Voigt, H. Schlager, and P. Popp: A climatological view to HNO₃
12 partitioning in cirrus clouds, *Q. J. R. Meteorol. Soc.*, 134, 905–912, doi:10.1002/qj.253,
13 2008.
- 14 Keller, C. A., Long, M. S., Yantosca, R. M., Da Silva, A. M., Pawson, S., and Jacob, D. J.:
15 HEMCO v1.0: a versatile, ESMF-compliant component for calculating emissions in
16 atmospheric models, *Geosci. Model Dev.*, 7, 1409–1417, [https://doi.org/10.5194/gmd-7-](https://doi.org/10.5194/gmd-7-1409-2014)
17 [1409-2014](https://doi.org/10.5194/gmd-7-1409-2014), 2014.
- 18 Kinne, S., Schulz, M., Textor, C., Guibert, S., Balkanski, Y., Bauer, S. E., Berntsen, T., Berglen,
19 T. F., Boucher, O., Chin, M., Collins, W., Dentener, F., Diehl, T., Easter, R., Feichter, J.,
20 Fillmore, D., Ghan, S., Ginoux, P., Gong, S., Grini, A., Hendricks, J., Herzog, M.,
21 Horowitz, L., Isaksen, I., Iversen, T., Kirkevåg, A., Kloster, S., Koch, D., Kristjansson, J.
22 E., Krol, M., Lauer, A., Lamarque, J. F., Lesins, G., Liu, X., Lohmann, U., Montanaro, V.,
23 Myhre, G., Penner, J., Pitari, G., Reddy, S., Seland, O., Stier, P., Takemura, T., and Tie,
24 X.: An AeroCom initial assessment – optical properties in aerosol component modules of
25 global models, *Atmos. Chem. Phys.*, 6, 1815–1834, [https://doi.org/10.5194/acp-6-1815-](https://doi.org/10.5194/acp-6-1815-2006)
26 [2006](https://doi.org/10.5194/acp-6-1815-2006), 2006.
- 27 Laakso, L., Grönholm, T., Rannik, U., Kosmale, M., Fiedler, V., Vehkamäki, H., and Kulmala,
28 M.: Ultrafine particle scavenging coefficients calculated from 6 years field measurements,
29 *Atmos. Environ.*, 37, 3605–3613, 2003.



- 1 Liu, H. Y., Jacob, D. J., Bey, I., and Yantosca, R. M.: Constraints from Pb-210 and Be-7 on wet
2 deposition and transport in a global three-dimensional chemical tracer model driven by
3 as-simulated meteorological fields, *J. Geophys. Res.-Atmos.*, 106,12109–12128, 2001.
- 4 Luo, G., Yu, F., and Schwab, J.: Revised treatment of wet scavenging processes dramatically
5 improves GEOS-Chem 12.0.0 simulations of surface nitric acid, nitrate, and ammonium
6 over the United States, *Geosci. Model Dev.*, 12, 3439–3447, [https://doi.org/10.5194/gmd-](https://doi.org/10.5194/gmd-12-3439-2019)
7 [12-3439-2019](https://doi.org/10.5194/gmd-12-3439-2019), 2019.
- 8 Mari, C., Jacob, D. J., and Bechtold, P.: Transport and scavenging of soluble gases in a deep
9 convective cloud, *J. Geophys. Res.*, 105 (D17), 22255–22267,
10 [doi:10.1029/2000JD900211](https://doi.org/10.1029/2000JD900211), 2000.
- 11 Martin, R. V., Jacob, D. J., Yantosca, R. M., Chin, M., and Ginoux, P.: Global and regional
12 decreases in tropospheric oxidants from photochemical effects of aerosols, *J. Geophys.*
13 *Res.*, 108, 4097, [doi:10.1029/2002JD002622](https://doi.org/10.1029/2002JD002622), D3, 2003.
- 14 Moch, J. M., Dovrou, E., Mickley, L. J., Keutsch, F. N., Cheng, Y., Jacob, D. J., Jiang, J., Li, M.,
15 Munger, J. W., Qiao, X. and Zhang, Q.: Contribution of Hydroxymethane Sulfonate to
16 Ambient Particulate Matter: A Potential Explanation for High Particulate Sulfur During
17 Severe Winter Haze in Beijing, *Geophysical Research Letters*, 45(21), 11,969-11,979,
18 [doi:10.1029/2018GL079309](https://doi.org/10.1029/2018GL079309), 2018.
- 19 Moch, J.M., Mickley, L.J., Jacob, D.J., Dovrou, E., Keutsch, F.N., Alexander, B., Cheng, Y.,
20 Jiang, J., Li, M., Munger, J.W., Shao, J., Qiao, X., and Zhang, Q.,: Hydroxymethane
21 sulfonate in extreme haze: Initial results from GEOS-Chem, 9th International GEOS-
22 Chem Meeting, Cambridge, Massachusetts, USA, May 6-9, 2019.
- 23 Myhre, G., Samset, B. H., Schulz, M., Balkanski, Y., Bauer, S., Berntsen, T. K., Bian, H.,
24 Bellouin, N., Chin, M., Diehl, T., Easter, R. C., Feichter, J., Ghan, S. J., Hauglustaine, D.,
25 Iversen, T., Kinne, S., Kirkevåg, A., Lamarque, J.-F., Lin, G., Liu, X., Lund, M. T., Luo,
26 G., Ma, X., van Noije, T., Penner, J. E., Rasch, P. J., Ruiz, A., Seland, Ø., Skeie, R. B.,
27 Stier, P., Takemura, T., Tsigaridis, K., Wang, P., Wang, Z., Xu, L., Yu, H., Yu, F., Yoon,
28 J.-H., Zhang, K., Zhang, H., and Zhou, C.: Radiative forcing of the direct aerosol effect
29 from AeroCom Phase II simulations, *Atmos. Chem. Phys.*, 13, 1853–1877,
30 <https://doi.org/10.5194/acp-13-1853-2013>, 2013.
- 31 Nenow D.: Surface premelting. *Prog. Crystal Growth Char* 9, 185-225, 1984.



- 1 Niedermeier, D., S. Augustin-Bauditz, S. Hartmann, H. Wex, K. Ignatius, and F. Stratmann: Can
2 we define an asymptotic value for the active surface site density for heterogeneous ice
3 nucleation? *J. Geophys. Res. Atmos.*, 120, 5036–5046, doi:10.1002/2014JD022814, 2015.
- 4 Ocampo J. and Klinger J.: Modification of the surface structure of ice during aging *J. phys.*
5 *Chem.* 87, 4167-4170, 1983.
- 6 Pandis, S. N., and Seinfeld, J. H.: Sensitivity analysis of a chemical mechanism for
7 aqueous - phase atmospheric chemistry, *J. Geophys. Res.*, 94(D1), 1105– 1126,
8 doi:10.1029/JD094iD01p01105, 1989.
- 9 Penner, J.E., R.J. Charlson, J.M. Hales, N.S. Laulainen, R. Leifer, T. Novakov, J. Ogren, L.F.
10 Radke, S.E. Schwartz, and L. Travis: Quantifying and Minimizing Uncertainty of
11 Climate Forcing by Anthropogenic Aerosols. *Bull. Amer. Meteor. Soc.*, 75, 375–400,
12 [https://doi.org/10.1175/1520-0477\(1994\)075<0375:QAMUOC>2.0.CO;2](https://doi.org/10.1175/1520-0477(1994)075<0375:QAMUOC>2.0.CO;2), 1994
- 13 Rosenfeld, D., W.L. Woodley: Deep convective clouds with sustained highly supercooled liquid
14 water until -37.5°C. *Nature*, 405,440-442, 2000.
- 15 Sassen, K.: Supercooled Liquid Water In Winter Storms: A Preliminary Climatology from
16 Remote Sensing Observations, *J. Wea. Mod.*, 17, 30-35, 1985.
- 17 Schneider, A., Flanner, M., De Roo, R., and Adolph, A.: Monitoring of snow surface near-
18 infrared bidirectional reflectance factors with added light-absorbing particles, *The*
19 *Cryosphere*, 13, 1753–1766, <https://doi.org/10.5194/tc-13-1753-2019>, 2019.
- 20 Seinfeld, J.H. and Pandis, S.N.: *Atmospheric Chemistry and Physics: From Air Pollution to*
21 *Climate Change*. John Wiley & Sons, Hoboken, 2016.
- 22 Shiraiwa, M., Ueda, K., Pozzer, A., Lammel, G., Kampf, C. J., Fushimi, A., Enami, S., Arangio,
23 A. M., Fröhlich-Nowoisky, J., Fujitani, Y., Furuyama, A., Lakey, P. S. J., Lelieveld, J.,
24 Lucas, K., Morino, Y., Pöschl, U., Takahama, S., Takami, A., Tong, H., Weber, B.,
25 Yoshino, A., and Sato, K.: Aerosol Health Effects from Molecular to Global Scales,
26 *Environ. Sci. Technol.*, 51, 13545–13567, <https://doi.org/10.1021/acs.est.7b04417>, 2017.
- 27 Silvern, R. F., Jacob, D. J., Kim, P. S., Marais, E. A., Turner, J. R., Campuzano-Jost, P., and
28 Jimenez, J. L.: Inconsistency of ammonium–sulfate aerosol ratios with thermodynamic
29 models in the eastern US: a possible role of organic aerosol, *Atmos. Chem. Phys.*, 17,
30 5107–5118, <https://doi.org/10.5194/acp-17-5107-2017>, 2017.



- 1 Smith, R.M. and Martell, A.E.: Critical Stability Constants, Vol. 2, Amine Complexes, Plenum
2 Publ., Co., New York, 1976.
- 3 Strom, J., B. Strauss, T. Anderson, F. Schroder, J. Heintzenberg, and P. Wendhng: In situ
4 observations of the microphysical properties of young cirrus clouds, *J. Atmos. Sci.*, 541,
5 2542-2553, 1997.
- 6 Textor, C., Schulz, M., Guibert, S., Kinne, S., Balkanski, Y., Bauer, S., Bernsten, T., Berglen, T.,
7 Boucher, O., Chin, M., Dentener, F., Diehl, T., Easter, R., Feichter, H., Fillmore, D.,
8 Ghan, S., Ginoux, P., Gong, S., Grini, A., Hendricks, J., Horowitz, L., Huang, P., Isaksen,
9 I., Iversen, I., Kloster, S., Koch, D., Kirkevåg, A., Kristjansson, J. E., Krol, M., Lauer, A.,
10 Lamarque, J. F., Liu, X., Montanaro, V., Myhre, G., Penner, J., Pitari, G., Reddy, S.,
11 Seland, Ø., Stier, P., Takemura, T., and Tie, X.: Analysis and quantification of the
12 diversities of aerosol life cycles within AeroCom, *Atmos. Chem. Phys.*, 6, 1777–1813,
13 <https://doi.org/10.5194/acp-6-1777-2006>, 2006.
- 14 Turnock, S. T., Mann, G. W., Woodhouse, M. T., Dalvi, M., O'Connor, F. M., Carslaw, K. S., &
15 Spracklen, D. V.: The impact of changes in cloud water pH on aerosol radiative forcing.
16 *Geophysical Research Letters*, 46, 4039– 4048. <https://doi.org/10.1029/2019GL082067>,
17 2019.
- 18 Voigt, C., Schlager, H., Ziereis, H., Krämer, B., Luo, B. P., Schiller, C., Krämer, M., Popp, P. J.,
19 Irie, H., and Kondo, Y.: Nitric acid in cirrus clouds, *Geophys. Res. Lett.*, 33, L05803, doi:
20 10.1029/2005GL025159, 2006.
- 21 Walcek, C.J. and G.R. Taylor: A Theoretical Method for Computing Vertical Distributions of
22 Acidity and Sulfate Production within Cumulus Clouds. *J. Atmos. Sci.*, 43, 339–355,
23 [https://doi.org/10.1175/1520-0469\(1986\)043<0339:ATMFCV>2.0.CO;2](https://doi.org/10.1175/1520-0469(1986)043<0339:ATMFCV>2.0.CO;2), 1986.
- 24 Wang, Q., Jacob, D. J., Fisher, J. A., Mao, J., Leibensperger, E. M., Carouge, C. C., Le Sager, P.,
25 Kondo, Y., Jimenez, J. L., Cubi-son, M. J., and Doherty, S. J.: Sources of carbonaceous
26 aerosols and deposited black carbon in the Arctic in winter-spring: implications for
27 radiative forcing, *Atmos. Chem. Phys.*, 11, 12453–12473, [https://doi.org/10.5194/acp-11-](https://doi.org/10.5194/acp-11-12453-2011)
28 12453-2011, 2011.
- 29 Wang, Q., Jacob, D. J., Spackman, J. R., Perring, A. E., Schwarz, J.P., Moteki, N., Marais, E. A.,
30 Ge, C., Wang, J., and Barrett, S. R.H.: Global budget and radiative forcing of black



- 1 carbon aerosol: constraints from pole-to-pole (HIPPO) observations across the Pacific, J.
2 Geophys. Res., 119, 195–206, 2014
- 3 Wang, X., Zhang, L., and Moran, M. D.: Uncertainty assessment of current size-resolved
4 parameterizations for below-cloud particle scavenging by rain, Atmos. Chem. Phys., 10,
5 5685–5705, <https://doi.org/10.5194/acp-10-5685-2010>, 2010.
- 6 Wang, X., Zhang, L., and Moran, M. D.: Development of a new semi-empirical parameterization
7 for below-cloud scavenging of size-resolved aerosol particles by both rain and snow,
8 Geosci. Model Dev., 7, 799–819, <https://doi.org/10.5194/gmd-7-799-2014>, 2014.
- 9 Wesely, M. L.: Parameterization of surface resistances to gaseous dry deposition in regional-
10 scale numerical models, Atmos. Environ., 23, 1293–1304, 1989.
- 11 Wesely, M. L., Sisterson, D. L., and Jastrow, J. D.: Observations of the chemical properties of
12 dew on vegetation that affect the dry deposition of SO₂, J. Geophys. Res., 95, 7501–7514,
13 1990.
- 14 Yu, F. and Luo, G.: Simulation of particle size distribution with a global aerosol model:
15 contribution of nucleation to aerosol and CCN number concentrations, Atmos. Chem.
16 Phys., 9, 7691–7710, [doi:10.5194/acp-9-7691-2009](https://doi.org/10.5194/acp-9-7691-2009), 2009.
- 17 Yu, F., Luo, G., and Ma, X.: Regional and global modeling of aerosol optical properties with a
18 size, composition, and mixing state resolved particle microphysics model, Atmos. Chem.
19 Phys., 12, 5719–5736, <https://doi.org/10.5194/acp-12-5719-2012>, 2012.



Table 1. List of Λ and b values for rain and snow washout parameterizations.

	Rain		Snow	
	T>268 K		248 K<T<268 K	
	Λ	b	Λ	b
GC12				
HNO ₃	2.8×10^{-5}	1.0	0	0
Coarse aerosol	2.6×10^{-4}	0.79	4.2×10^{-4}	0.96
Fine aerosol	4.3×10^{-6}	0.61	8.8×10^{-6}	0.96
This work				
HNO ₃	$3 \times 10^{-3} \ddagger$	$0.62 \ddagger$	$3 \times 10^{-3} \ddagger$	$0.62 \ddagger$
Coarse aerosol	$2 \times 10^{-4} \dagger$	$0.85 \dagger$	$2 \times 10^{-3} \dagger$	$0.7 \dagger$
Hydrophobic fine aerosol	$5 \times 10^{-7} \dagger$	$0.7 \dagger$	$1 \times 10^{-5} \dagger$	$0.66 \dagger$
Hydrophilic fine aerosol	$1 \times 10^{-5} *$	$0.7 \dagger$	$2 \times 10^{-4} *$	$0.66 \dagger$

[†] from Wang et al. (2014) assuming fine aerosol with diameter of 100 nm and coarse aerosol with diameter of 6 μm ; [‡] from Luo et al. (2019); ^{*} this work.



Table 2. Observed annual mean surface concentrations of aerosol precursors and aerosols over the US, Europe, and East Asia. Annual mean surface concentrations (M , $\mu\text{g m}^{-3}$), normalized mean bias (NMB, %), and correlation coefficient (r , when # of samples > 10) between observed and simulated annual mean values for the 8 species by G12, L2019, and WETrev cases.

	USA			Europe			Asia		
	G12	L2019	WETrev	G12	L2019	WETrev	G12	L2019	WETrev
SO2	M: 5.61 NMB	4.48 -20	4.33 -23	M: 1.36 NMB	2.72 101	2.50 84	M: 2.51 NMB	4.08 63	3.58 43
	r	0.49	0.48	r	0.56	0.55	r		
HNO3	M: 0.83 NMB	1.47 78	0.93 13	M: 0.67 NMB	1.05 56	0.51 -24	M: 0.86 NMB	1.90 121	0.64 -26
	r	0.57	0.59	r			r		
NH3	M: 1.00 NMB	1.02 2.6	1.18 19	M: 0.83 NMB	1.11 33	1.13 35	M: 0.96 NMB	0.95 -1.7	0.88 -8.6
	r	0.26	0.29	r	0.85	0.84	r		
SO4	M: 1.30 NMB	1.29 -1.1	1.15 -11	M: 1.29 NMB	1.64 27	1.05 -18	M: 2.63 NMB	2.77 5.5	1.69 -36
	r	0.92	0.92	r	0.92	0.91	r		
NIT	M: 0.71 NMB	1.60 126	0.88 24	M: 1.66 NMB	3.42 105	1.43 -14	M: 0.60 NMB	2.23 269	0.89 47
	r	0.53	0.61	r	0.83	0.83	r		
NH4	M: 0.61 NMB	0.89 45	0.65 6.2	M: 0.88 NMB	1.68 91	0.85 -3.3	M: 0.58 NMB	1.55 167	0.82 42
	r	0.76	0.79	r	0.79	0.80	r		
BC	M: 0.20 NMB	0.18 -7.0	0.17 -14	M: 0.51 NMB	0.38 -25	0.32 -37			
	r	0.54	0.54	r					
OC	M: 1.01 NMB	0.80 -20	0.72 -29	M: 1.97 NMB	1.00 -49	0.77 -61			
	r	0.63	0.65	r					

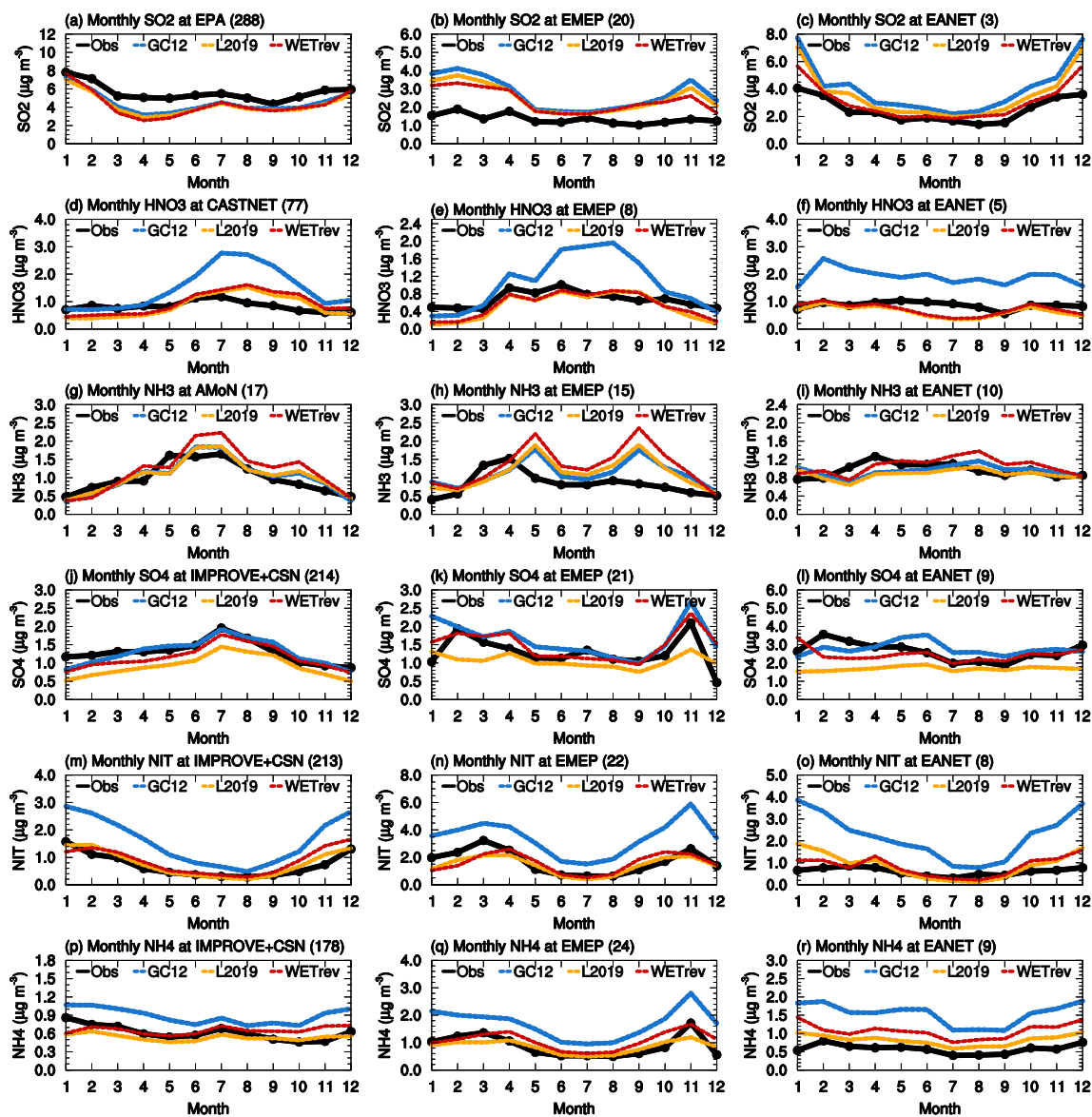


Figure 1. Variations of monthly means for year 2011 showing the comparisons of sulfur dioxide, nitric acid, ammonia, sulfate, nitrate, and ammonium surface mass concentrations which are observed over (left column) the United States, (center column) Europe, and (right column) East Asia sites (black) and simulated by GC12 (blue), L2019 (yellow), and WETrev (red) cases.

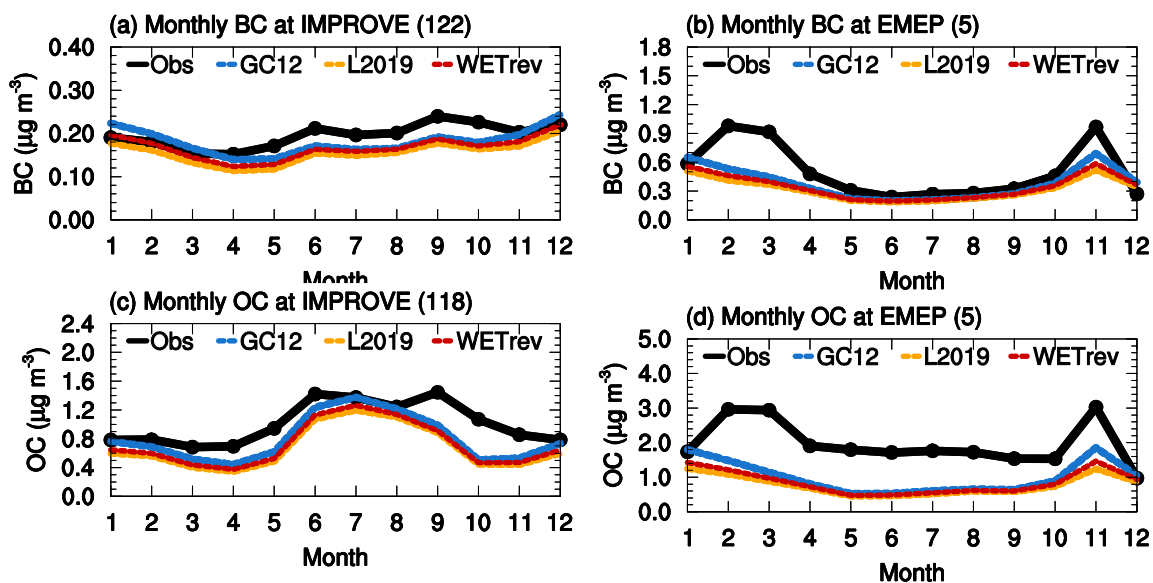


Figure 2. Variations of monthly means for year 2011 showing the comparisons of black carbon and organic carbon surface mass concentrations which are observed over (left column) the United States and (right column) Europe sites (black) and simulated by GC12 (blue), L2019 (yellow), and WETrev (red) cases.

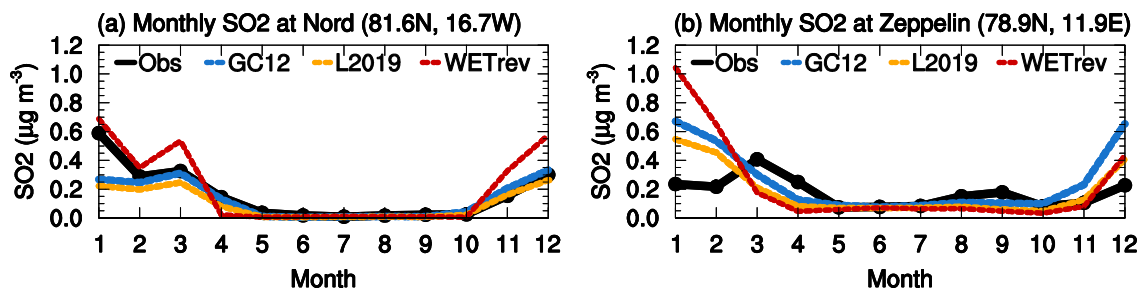


Figure 3. Variations of multiyear monthly means showing the comparisons of sulfur dioxide surface mass concentrations which are observed (2008-2013) at (a) Nord (2008-2013) and (b) Zeppelin () sites (black) and simulated (2011) by GC12 (blue), L2019 (yellow), and WETrev (red) cases.

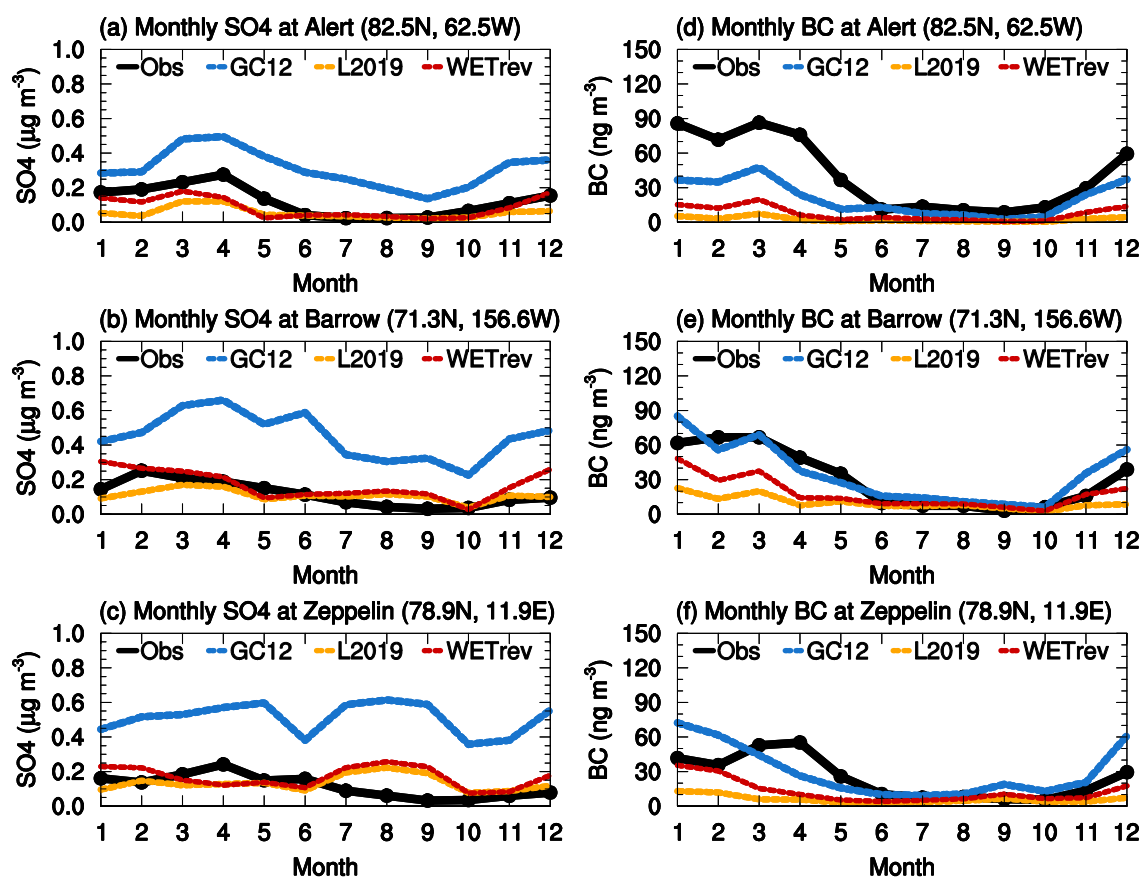


Figure 4. Variations of multiyear monthly means showing the comparisons of (a-c) sulfate and (d-f) black carbon surface mass concentrations which are observed at (top) Alert (2008-2012), (middle) Barrow (2008-2013), and (bottom) Zeppelin (2008-2013) sites (black) and simulated (2011) by GC12 (blue), L2019 (yellow), and WETrev (red) cases.

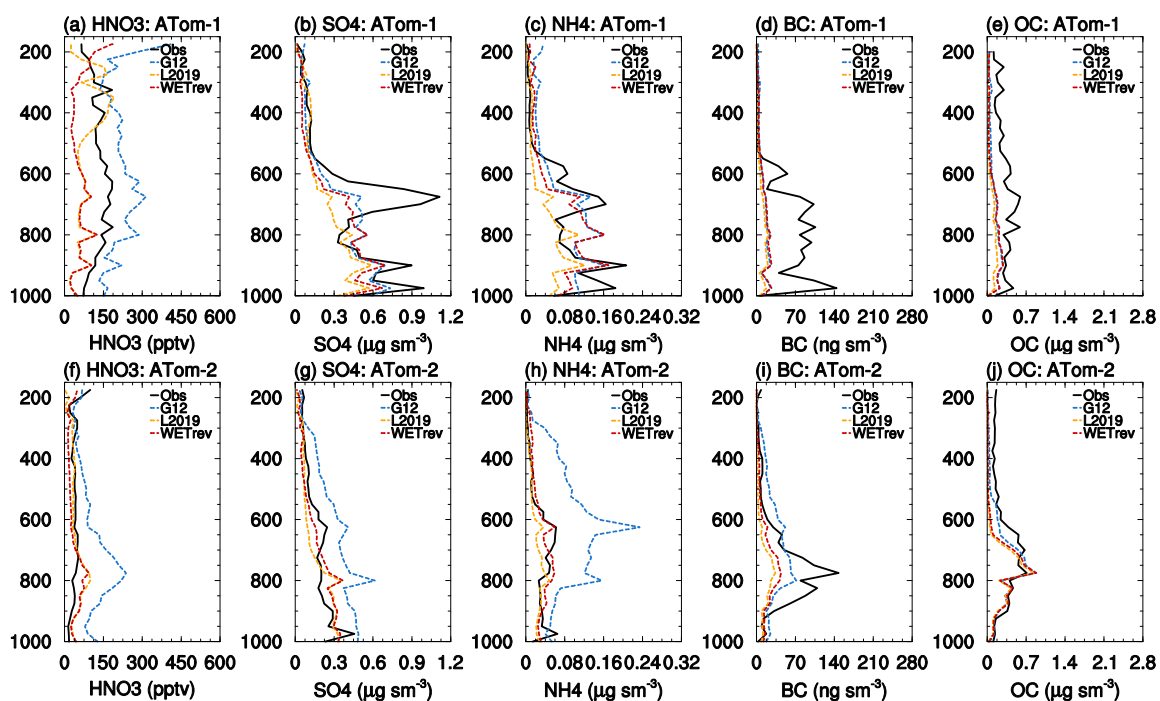


Figure 5. Vertical profiles of nitric acid, sulfate, ammonium, black carbon, and organic carbon from ATom aircraft observations (black, ATom-1: a-e; ATom-2: f-j) and GEOS-Chem simulations by GC12 (blue), L2019 (yellow) and WETrev (red) cases over the North hemisphere.

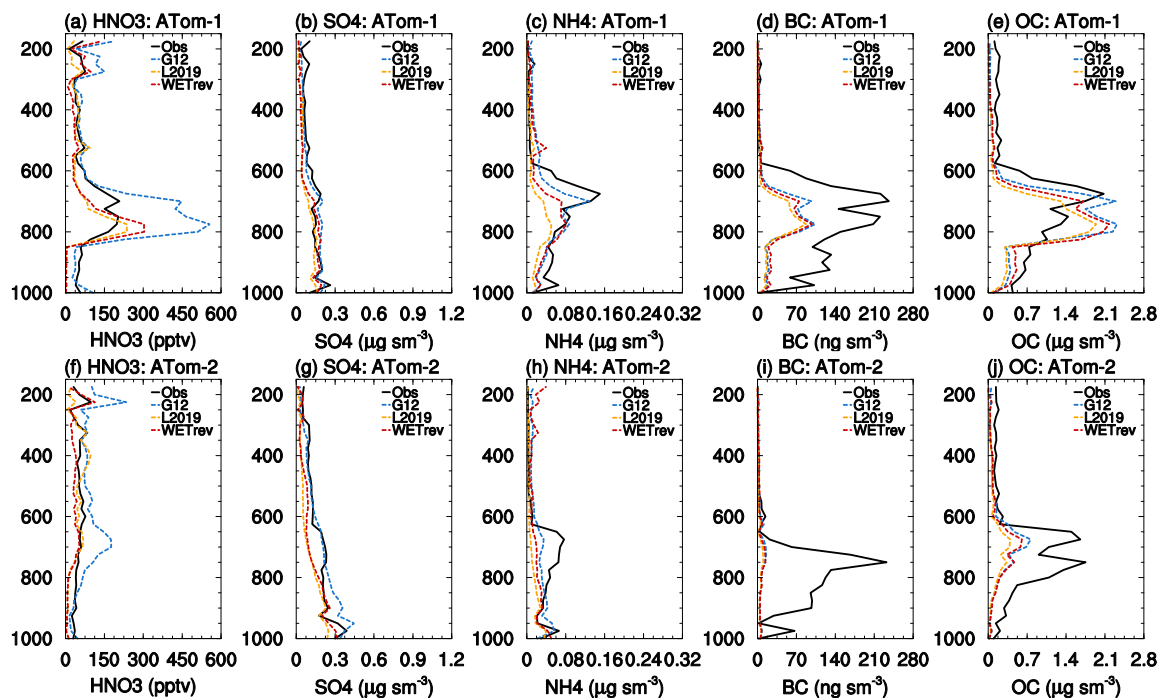


Figure 6. The same as Fig 5. but over the South Hemisphere.

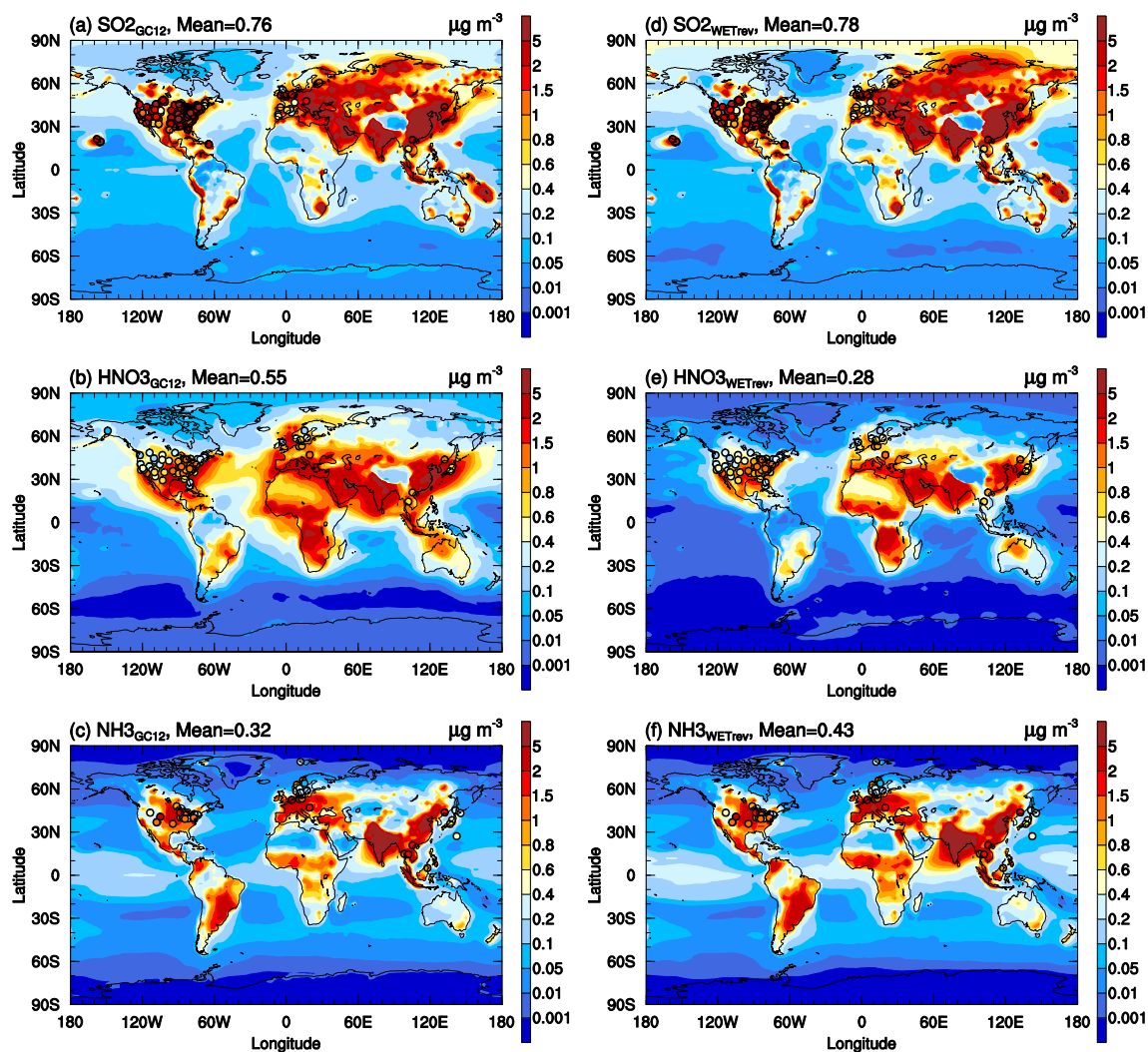


Figure 7. Horizontal distributions of sulfur dioxide, nitric acid, and ammonia surface mass concentrations simulated by (a-c) GC12 case and (d-f) WETrev case. Filled circles are annual mean surface mass concentrations observed at IMPROVE, CSN, CASTNET, AMoN, EMEP, and EANET for corresponding species.

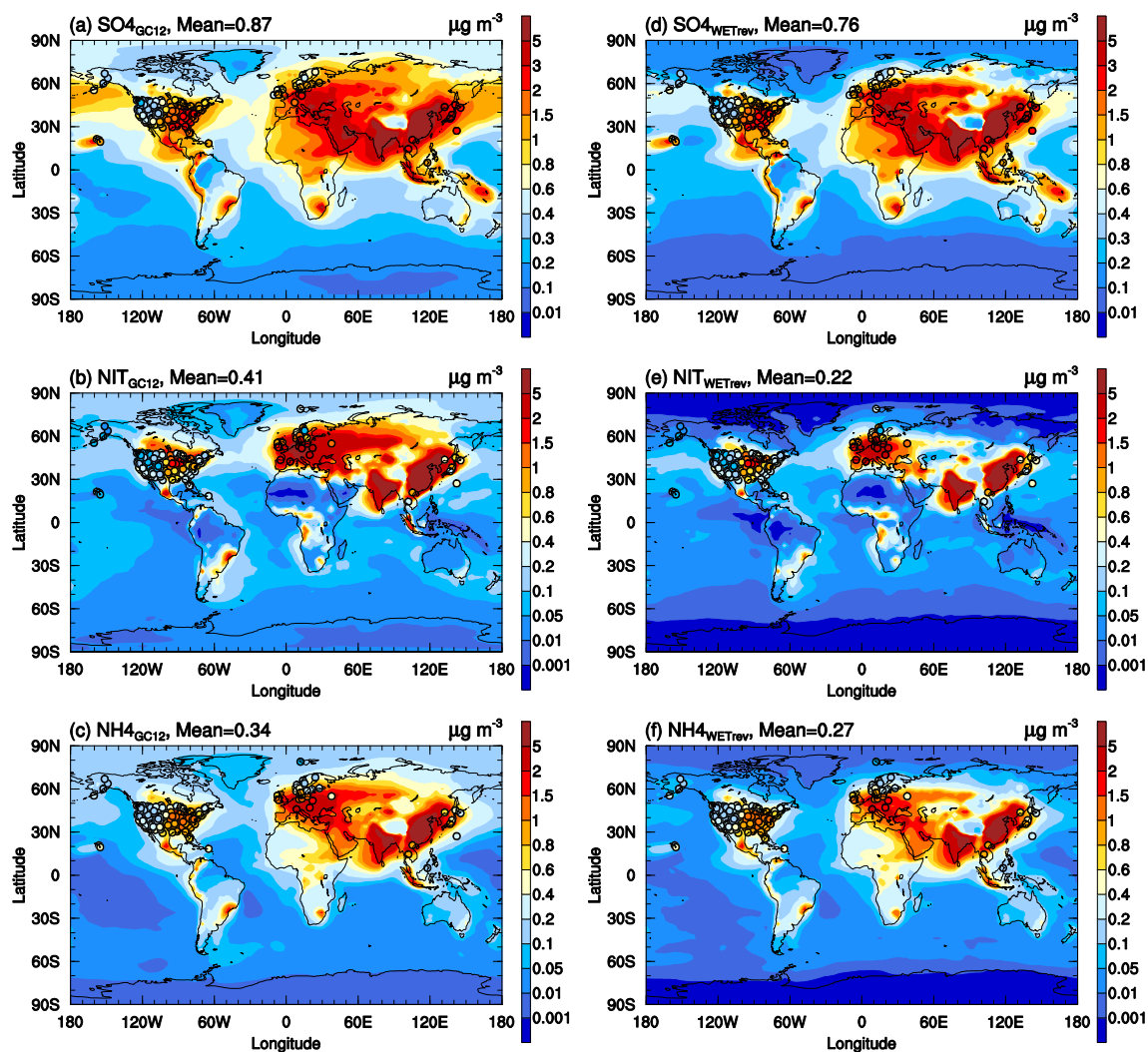


Figure 8. The same as Fig. 7 but for sulfate, nitrate, and ammonium surface mass concentrations.

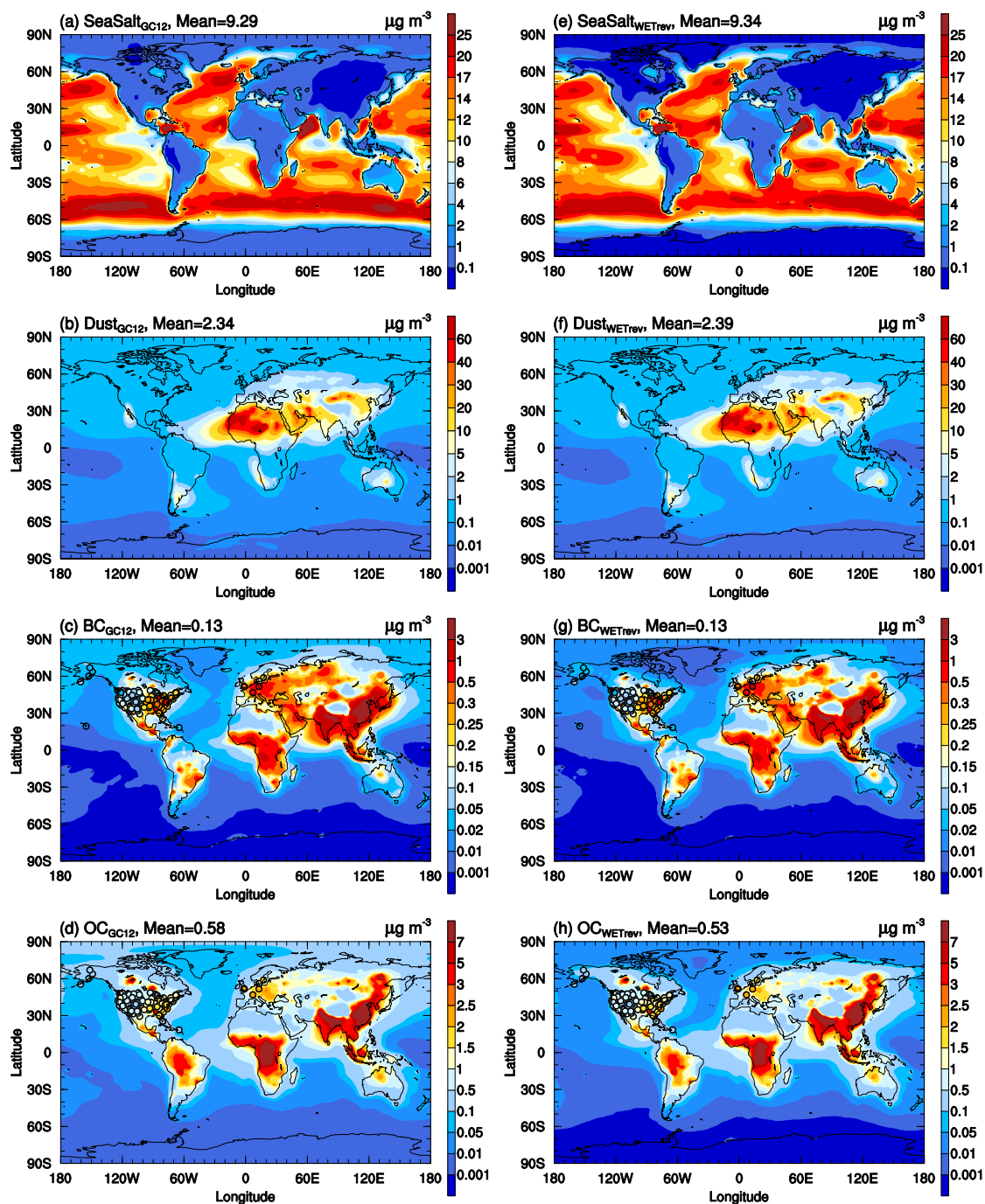


Figure 9. The same as Fig. 7 but for black carbon, organic carbon, sea salt, and dust surface mass concentrations.

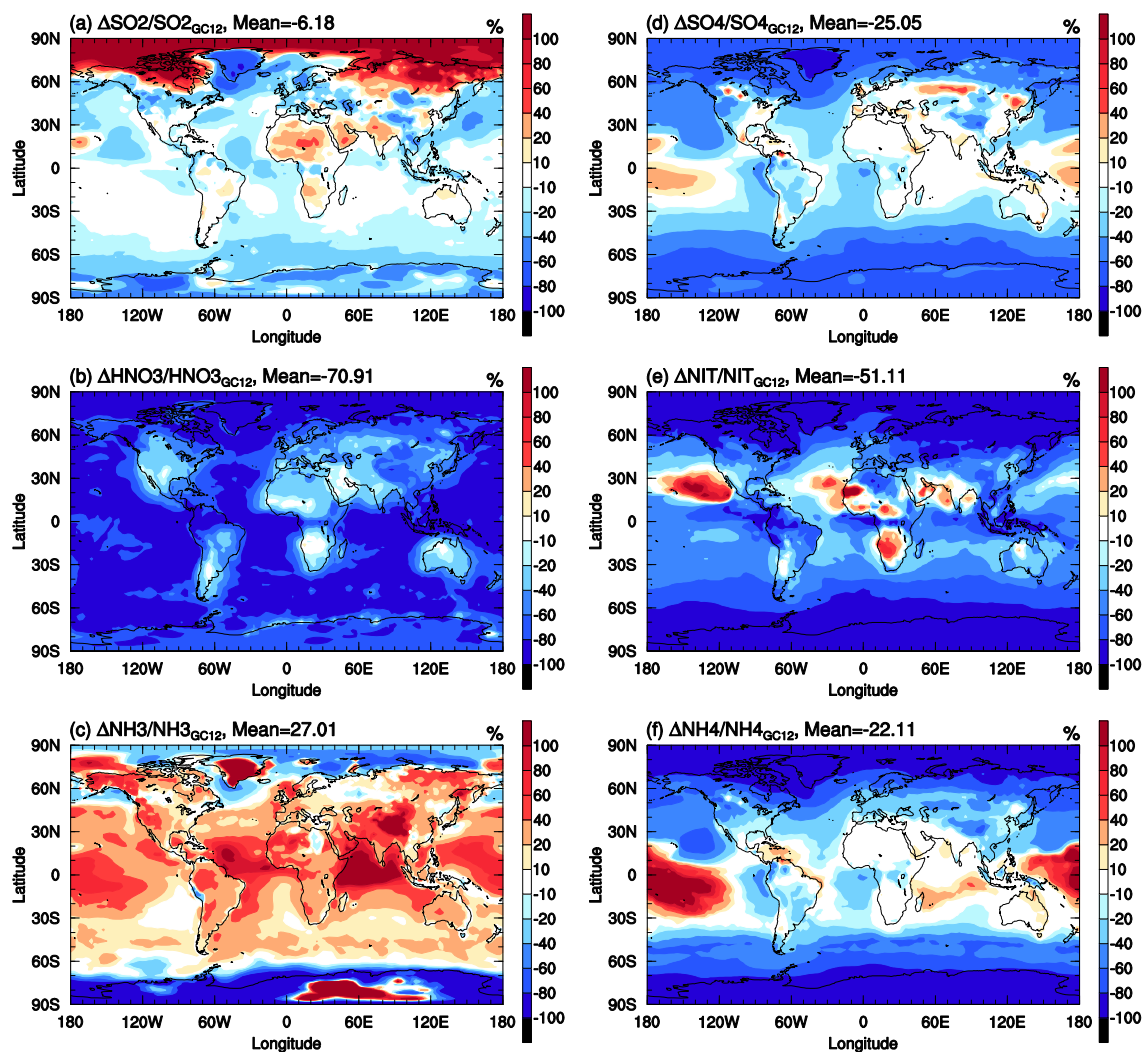


Figure 10. Horizontal distributions of percentage changes in annual mean (a) sulfur dioxide, (b) nitric acid, (c) ammonia, (d) sulfate, (e) nitrate, and (f) ammonium surface mass concentrations due to the switching of GC12 case to WETrev case.

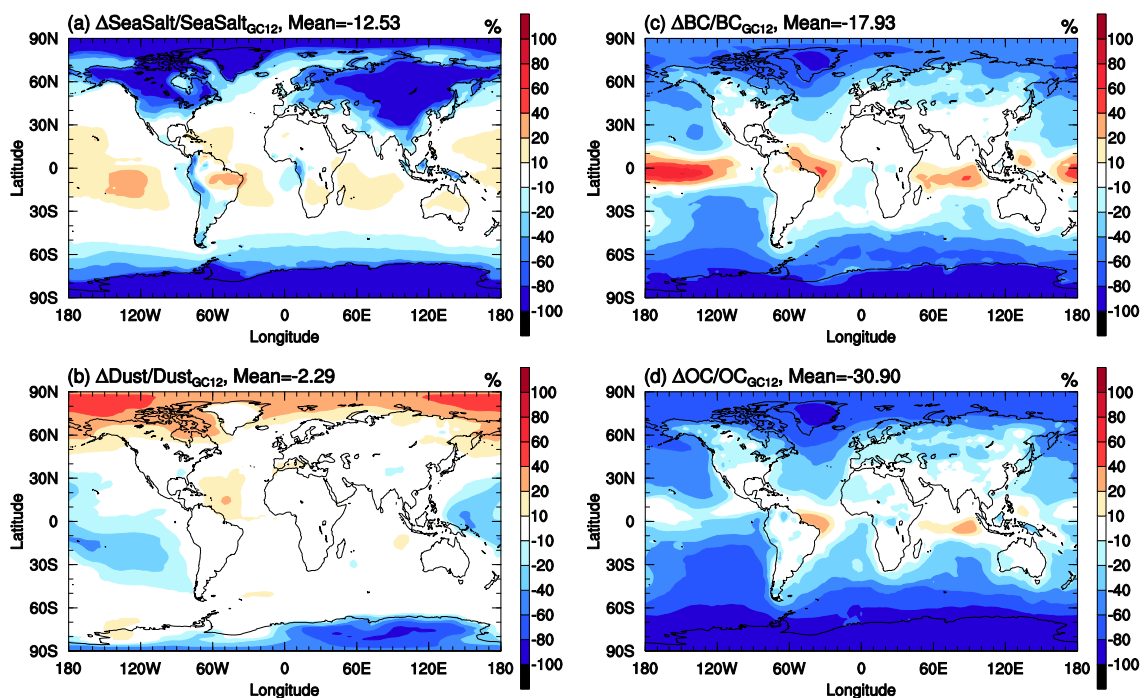


Figure 11. The same as Fig. 10 but for black carbon, organic carbon, sea salt, and dust surface mass concentrations.